



TECHNISCHE  
UNIVERSITÄT  
WIEN

VIENNA  
UNIVERSITY OF  
TECHNOLOGY

## DIPLOMARBEIT

# Stabilized source of entangled photon pairs characterized by quantum state tomography

Ausgeführt am  
Atominstitut der technischen Universität Wien

unter Anleitung von **Univ. Doz. DI Dr. Martin Suda**

in Zusammenarbeit mit dem

Austrian Institute of Technology  
Betreuer: **DI Dr. Andreas Poppe**

durch

**Florian Bruckner**  
Vitiser Straße 45/4  
A-3830 Waidhofen/Th.

November 30, 2009

---

Datum

---

Unterschrift



## **Abstract**

Today there exist many applications for entangled photon pairs. Quantum cryptography, quantum information and quantum computation are the most important research areas that make use of quantum entanglement. The aim of this diploma thesis is to provide an easy to use entangled photon source for such applications. Finally the source should be fully automated and well characterized. During this work we implemented the first steps towards this final goal, namely a pump beam controller, automated fiber coupling, and an automated characterization by a quantum state tomography.



# Contents

<b>1</b>	<b>Introduction</b>	<b>1</b>
1.1	Motivation	1
1.2	Overview	2
1.3	Acknowledge	2
<b>2</b>	<b>Theory</b>	<b>3</b>
2.1	Gaussian beams	3
2.1.1	Working with ABCD-matrices using MAPLE	5
2.2	Entanglement	7
2.2.1	Definition	7
2.2.2	The Bell states	7
2.2.3	Some entanglement measures	8
2.2.4	Applications	9
2.3	Spontaneous Parametric Down-Conversion	12
2.3.1	Type II	13
2.3.2	Type I	13
2.3.3	Optimal Coupling	14
2.3.4	Walkoff Compensation	14
2.4	The Poincare sphere	15
2.5	Quantum state tomography	17
2.5.1	Maximum likelihood technique	17
2.5.2	Systematic errors	18
2.5.3	Number of detectors to use	19
<b>3</b>	<b>Source Design</b>	<b>21</b>
3.1	Laser Violet-405 from Oxxius	22
3.1.1	Measurement of the power control feature	22
3.1.2	Measurement of the laser spectrum	23
3.1.3	Measurement of the beam profile	24
3.2	Focusing Optics	25
3.2.1	Theoretical considerations	25
3.2.2	Simulation	26
3.2.3	Practical considerations	26
3.2.4	The Result	27
3.2.5	Comparison with the original laser system	29
3.2.6	Future development	29
3.3	Beam Control Loop	30
3.3.1	The 4-quadrant-diode PDQ80A	30
3.3.2	The Labjack USB-ADC U3-HV	31
3.3.3	The Agilis-mirror-mounts	32
3.3.4	The Agilis-controller UG-AC2 (UG-AC8)	32
3.3.5	Sensitivity measurement	33
3.3.6	The control algorithm	35
3.3.7	Future development	36
3.4	Pair creation and walkoff compensation	37
3.4.1	Theoretical considerations	37
3.4.2	Practical considerations	37
3.4.3	Measurement of the ring system	37
3.4.4	BBO characteristics	38
3.5	Coupling Optics	39
3.5.1	Theoretical considerations	39
3.5.2	Practical considerations	40
3.5.3	Automated coupling	41
3.5.4	Measurement of the coupled beam profile	42

3.5.5	Comparison with the original coupling system . . . . .	43
3.5.6	Future development . . . . .	43
<b>4</b>	<b>Measurement system</b>	<b>45</b>
4.1	Single photon detectors . . . . .	45
4.1.1	Measurement of the detector offsets . . . . .	47
4.2	The timetagging module TTMS . . . . .	47
4.2.1	Hardware . . . . .	48
4.2.2	Software . . . . .	48
4.3	The quantum state tomography stage . . . . .	51
4.3.1	Design . . . . .	51
4.3.2	Motorized rotation stages . . . . .	53
4.3.3	Waveplate adjustment . . . . .	55
4.4	Analysis software . . . . .	56
4.4.1	Data acquisition . . . . .	56
4.4.2	Computation . . . . .	57
4.5	Measurements . . . . .	59
4.5.1	Aligned system . . . . .	59
4.5.2	Misaligned system . . . . .	60
4.6	Future development . . . . .	60
<b>5</b>	<b>Conclusion</b>	<b>61</b>
5.1	Laser system . . . . .	61
5.2	Beam control . . . . .	61
5.3	Walkoff compensation . . . . .	61
5.4	Coupling system . . . . .	62
5.5	Quantum state tomography . . . . .	62
<b>A</b>	<b>Example calculation with MAPLE</b>	<b>63</b>
A.1	Include Packages . . . . .	63
A.2	Function Definitions . . . . .	63
A.3	Initial Beam . . . . .	63
A.4	Direct map . . . . .	63
A.5	Map with intermediate focus . . . . .	64
A.6	Calculation . . . . .	64
<b>B</b>	<b>Setup HowTo for Agilis controller AG-UC2</b>	<b>65</b>
B.1	setup_howto.txt . . . . .	65
B.2	AG_UC2_cmd expect scripts . . . . .	66

# 1 Introduction

Quantum physics is one of the most successful theories in the history of physics. Some very small quantum effects lead to an unexpected macroscopic behaviour that can only be described by quantum theory. In recent years it became feasible to directly measure these quantum effects and not only their implications. And it is not only possible to measure quantum states but also to prepare a initial states and perform some operations with them. This allows to make use of quantum effects in order to solve some specific problems more efficiently. Currently research in this topic is still in its infancy. It is possible to handle only a few quantum objects at a time, but this is enough to demonstrate the correctness of quantum physics and all of its implications.

The problem with these quantum objects is that they are very sensitive to environmental influences. Every measurement even every interaction leads to a change of the system state and could destroy entanglement or superpositions. This is also the reason why we don't experience quantum physics in our every day life. Because we are embedded in our environment all macroscopic objects are exposed to many interactions and therefore all quantum effects are destroyed. Even for very small particles it is very complicated to shield them from the environment.

One possibility to solve this problem is to use weakly interacting particles as in our case photons. In vacuum these particles do not interact with each other at all, but within a crystal it is possible to reach an effective interaction and create entangled photon pairs. Since this interaction is very unlikely this means that if an entangled pair is created it is also stable for a long time. Additionally photons of a certain wavelength are well suited for long range transmission using standard telecom fibers. The big problem with using photons is that due to the missing interaction they are not easy to control and since they are moving objects it is not possible to store them. Precise knowledge of the coherence is needed in order to let two photons interact with each other. Only if they meet at an optical element within a very small time window there would be a measurable effect.

Another way to implement the quantum system would be to use atoms or ions. Since these particles are affected by the electromagnetic force it is easier to control them. The needed interactions to realize some quantum operations can be applied at any time which makes the handling much more flexible. On the other hand these particles are also coupled to the environment over the electromagnetic force. Although one tries to shield this unwanted interaction as good as possible it anyhow leads to decoherence after some time. Nevertheless for calculation in large quantum computers these systems would be preferred because they better scale for large particle numbers.

For future quantum computers probably both of these systems are of importance. Easy to control particles for the actual computation and photons for quantum communication within the computer or with external receivers. Therefore the quantum interface between ions and photons is also a hot topic for current research.

## 1.1 Motivation

During this diploma thesis we developed and implemented a source of entangled photon pairs that can be used to demonstrate some of the basic quantum experiments as described in section [Applications](#). The main goal of this project was to re-implement an already known system ([1],[2]) with emphasis on the easy usability. Our intention was not to invent new principles of pair creation, but to build upon promising known concepts. Starting from this point we tried to spot the elements that make the practical usage of the source difficult and tried to improve them.

First of all this means to reduce as many degrees of freedom as possible. This can be achieved by a stable and compact setup that only allows to change those degrees of freedom that are necessary for the adjustment of the system. Furthermore one can then automate some of these remaining degrees of freedom by some control loops.

Another point that was very important for us was the characterization of the source. For the use of an

entangled photon source it should not be necessary to deal with the details of the source implementation, but there should be a detailed specification that fully describes the photon source. Such characteristic values are the coincidence rate, the ratio of coincidence rate and single rates, or the wavelength distribution of the photon pairs. Additionally the quality of entanglement is of special interest for most applications. But the measurement of entanglement requires a sequence of consecutive measurement in different bases - a so-called quantum state tomography. Automation of this otherwise time consuming task was another goal of this work.

## 1.2 Overview

This document is split into a theoretical and a practical part. The theoretical part at the beginning should explain some basics that are required to implement this entangled photon source as well as the quantum state tomography. Of course this part is only an overview over the concepts and techniques used and the interesting reader is referred to the literature given in the references section at the end of this document.

The practical section than handles all topics that are important for the practical implementation of the photon source as well as the quantum state tomography stage. It includes design criteria as well as measurements that show how these criteria were deduced. After the implementation of every part of the system we did some comparison measurements that allow to evaluate the new system. At the end of some sections I tried to give some intentions for future improvements.

Finally the conclusion section summarizes the results of the project and some parts of the project that are not directly related to the topic are mentioned in the appendix.

## 1.3 Acknowledge

I want to thank my advisors Andreas Poppe and Martin Suda for the possibility to accomplish this diploma thesis and for their help during the work. Additionally I want to give thanks to my colleagues from the Austrian Institute of Technology Thomas Lorünser, Edwin Querasser, Roland Lieger, Bernhard Ömer who lend me their support during different stages of the project.



## 2 Theory

This section contains the theoretical background that is necessary to understand our setup and what was needed to design it. I will try to create a useful source of information that proved necessary for me during development of the source. Of course I will also mention some very general concepts if it is needed for consistency reasons. As a book of reference about many different topics related to photonics I can recommend [3], whereas [4] gives a very profound introduction to quantum information theory.

### 2.1 Gaussian beams

A very useful concept for the calculation of lens systems are Gaussian beams. They describe the propagation of laser beams and how they are transformed by optical elements like lenses, mirrors and so on.

In our case we want to calculate a lens system that focuses the laser beam to a certain spot size in order to reach a maximal electrical field strength within the crystal that creates our photon pairs. A higher field strength will then lead to a more efficient pair creation process. So how can we calculate the lenses that we need for our setup?

The first step will be to model our input beam. And this is exactly where Gaussian beams come into play. A Gaussian beam is an approximate solution of Maxwell's equations if you make the paraxial approximation  $x^2 + y^2 \ll z^2$ . For a detailed calculation see [5]

The resulting beam looks like

$$\vec{E}(\vec{x}, t) = A(\vec{x}) \vec{n} e^{-j(kz - \omega t)} \quad A(\vec{x}) = \frac{A_0}{q} e^{-jkr^2/2q} \quad (1)$$

where  $A(\vec{x})$  describes the radial beam profile with an amplitude  $A_0$  and a dependence on  $r$  the distance from the beam axis as well as on  $q$  which in turn depends on the  $z$  position. The polarization of the beam is given by the unit vector  $\vec{n}$ . In this representation the beam propagates in the  $z$ -direction with a wavevector  $k$  and a angular frequency  $\omega$ . See figures (1) and (2) and or a graphical illustration.

You see that the beam propagation is defined by one single parameter  $q$ . Which parameter you choose depends on the problem you want to solve. In the upper case it is  $q$  but there are also other parametrizations possible:

- **Complex parameter  $q$ :** For further calculation it has proved useful to use the complex beam parameter  $q(z) = z + jz_0$ . The imaginary part of this parameter is needed in order to avoid a singularity at  $q = 0$  and defines a certain beam width at the focus position  $z = 0$ . The real part then only defines the distance from this focus position.
- **Beam width  $w$ :** The whole beam with a wavelength  $\lambda$  is defined if you specify its focus location as well as the size of the beam at the focus (its beam waist). The size at every other  $z$  position can than be calculated as follows:

$$w(z) = w_0 \sqrt{1 + \left(\frac{z}{z_0}\right)^2} \quad z_0 = \frac{\pi w_0^2}{\lambda} \quad (2)$$

This value is very intuitive since you can directly measure it in your experimental setup using a CCD camera.

- **Rayleigh range  $z_0$ , confocal parameter  $b$ :** In the upper formula we already used the Rayleigh range  $z_0$  which is the distance from the focus where the beam size is  $w_0\sqrt{2}$ . A similar and often used term is the confocal parameter that is simple twice the Rayleigh range:  $b = 2z_0$ .
- **Beam divergence  $\theta$ :** The angle between the beam axis and its tangent for  $z \gg z_0$  is called beam divergence. The total angular spread of the beam is then simple two times the angle:

$$\theta \approx \frac{\lambda}{\pi w_0} \quad \Theta = 2\theta \quad (3)$$

The actual beam divergence can also be used to quantify the laser beam quality in practice, since a Gaussian beam has the smallest possible product of width and divergence. By measuring beam waist and far-field divergence in practice one is able to define the so-called  $M^2$  parameter that shows how much the real beam differs from an ideal Gaussian beam.

$$M^2 = \frac{\pi}{\lambda} \theta w_0 \quad M^2 > 1 \quad (4)$$

- **Other parameters:** Of course it is also possible to parametrize the Gaussian beam by any other value that can be mapped to one of the former parameters. Examples are the radius of curvature, the beam divergence, the Gouy phase and so on.

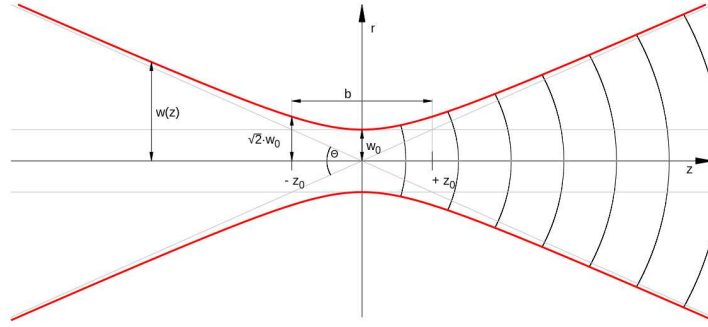


**FIGURE 1:** Example Gaussian beam to describe the upper parameters.

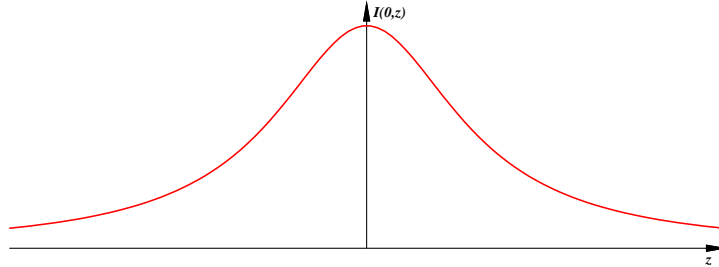


**FIGURE 2:** Intensity of a Gaussian beam on its axis depending on the distance from the focus point.

Using the complex parametrization described above one can define ray transfer matrices that model the action of many optical components. The complex vectors used to describe the beam looks like  $\begin{pmatrix} q \\ 1 \end{pmatrix}$  and the matrices are called ABCD matrices and look like  $\begin{pmatrix} A & B \\ C & D \end{pmatrix}$ . ABCD matrices can be multiplied as usual and new vectors can be obtained by the following simple relation:

$$\begin{pmatrix} q_2 \\ 1 \end{pmatrix} = k \begin{pmatrix} A & B \\ C & D \end{pmatrix} \begin{pmatrix} q_1 \\ 1 \end{pmatrix} \quad (5)$$

Solving the second line of the matrix equation for  $k$  and setting it in into the first line gives the following direct relation between  $q_2$  and  $q_1$ :

$$q_2 = \frac{Aq_1 + B}{Cq_1 + D} \quad (6)$$

The ABCD matrices of some important optical elements are listed in table (1). It is a bit surprising that these matrices match with that used in geometrical optics, but there are some differences that you have to

be aware of. Using Gaussian beams you will never be able to focus the beam to a dimensionless point as you mathematically could do in geometrical optics. This was achieved by the introduction of the imaginary part  $jz_0$  of the complex parameter  $q$ . Instead you have to bring to mind that the smaller the beam waist the smaller is also your  $z_0$  but the bigger is its divergence.

From this behaviour one can also deduce some very important practical facts. Namely if you want to focus a given input beam to a certain beam waist then you will experience that the smaller your beam waist is chosen the smaller becomes the distance of the focus from your lens. This can easily be seen when considering that the divergence angle is indirectly proportional to the beam waist.

Name	Matrix	Variable definition
Propagation	$\begin{pmatrix} 1 & d \\ 0 & 1 \end{pmatrix}$	$d = \text{distance}$
Refraction at a flat interface	$\begin{pmatrix} 1 & 0 \\ 0 & \frac{n_1}{n_2} \end{pmatrix}$	$n_{1,2} = \text{refractive indices}$
Reflection from a curved mirror	$\begin{pmatrix} 1 & 0 \\ -\frac{2}{R} & 1 \end{pmatrix}$	$R = \text{radius of curvature}$
Thin lens	$\begin{pmatrix} 1 & 0 \\ -\frac{1}{f} & 1 \end{pmatrix}$	$f = \text{focal length}$

**TABLE 1:** *List of some basic ABCD matrices*

In order to calculate more complex ABCD matrices or lens systems these basic matrices only have to be multiplied in the correct order. For example if a beam propagates a distance of  $a$ , then it is focused by a lens with focal length  $f$  and finally it further propagates a distance of  $b$ , the corresponding ABCD matrix could be calculated as follows:

$$\begin{pmatrix} 1 & b \\ 0 & 1 \end{pmatrix} \begin{pmatrix} 1 & 0 \\ -\frac{1}{f} & 1 \end{pmatrix} \begin{pmatrix} 1 & a \\ 0 & 1 \end{pmatrix} = \begin{pmatrix} 1 - \frac{b}{f} & a + b - \frac{ab}{f} \\ -\frac{1}{f} & 1 - \frac{a}{f} \end{pmatrix} \quad (7)$$

### 2.1.1 Working with ABCD-matrices using MAPLE

In order to calculate different lens systems it was useful to symbolically define generic beams and the ABCD matrices that connect these beams. To get your lens system you then have to define a set of constraints that your system has to fulfill. The number of conditions has to be equal to the number of degrees of freedom that you have. Using symbolical calculations also allows you to use derived values as constraints. In theory this procedure should get to the correct result for your lens system, but in practice there are some problems:

- **Nonlinearity:** Due to the fact that your problem is non-linear there is not a single solutions. The problems is that it is not easy to tell MAPLE which one is the physical solution (although it is possible to define some constraints using the `assume` command, these constraints are not considered by the numerical equation solver).
- **Numerical solver:** Solving the whole nonlinear system symbolically will not be possible for even small systems with 2 or 3 lenses. Thus we use a numerical solver if the problem cannot be solved symbolically. Using numerical algorithms does not guarantee that all solutions are found.

Despite these problems that inhibit the automated dimensioning of lens systems it proved useful to have a tool that allows you to define constraints and gives you the resulting lens system. If the whole system is too complicated it was possible to split the problem into some smaller parts for which it was possible to get explicit results. An easy example for such a MAPLE calculation can be found at [Example calculation with MAPLE](#).

So in order to create a very general framework that can be used to calculate any lens system I first defined a set of helper functions:

- **ABCD map:** This function maps an input beam into the beam that is created by some given ABCD matrix:

$$ABCD := (q, X) \rightarrow \frac{X[1, 1] \cdot q + X[1, 2]}{X[2, 1] \cdot q + X[2, 2]} \quad (8)$$

- **Create a lens' ABCD matrix:** This function maps a given focal length  $f$  to the 2-by-2 ABCD matrix of a thin lens:

$$L := (f) \rightarrow Matrix(2, 2, [[1, 0], [-1/f, 1]]) \quad (9)$$

- **Map a local  $q$  parameter to the corresponding beam width:** This function is needed because the beam waist is a one of the constraint that we want to determine for our lens system. Additionally this function is used in order to plot the beam profile.

$$w := (q, \lambda, M^2) \rightarrow \sqrt{M^2 \frac{\lambda}{\pi \cdot -Im(\frac{1}{q})}} \quad (10)$$

The positive  $M^2$  in this equation is a fit parameter that allows to fit the calculated functions to your measurement results. It means that the measured beam width in practice is always bigger than the calculated one. This is due to imperfections of the lenses. Unfortunately this adds new variables to our equation system that can only be measured in the final setup. Our problem is therefore not solvable any longer. Fortunately this  $M^2$  only has an influence on the beam width and thus only scales the final beam waist by a certain factor. And so we are able the correct the influence of the imperfect lens system by the lens position of the last lens.

If we now want to calculate a lens system we start with a definition of the input beam function  $q_0(z)$ . The first lens with focal length  $f_1$  is located at  $L_1$ , which means that we get the output beam at position  $L_1$  by applying the ABCD matrix on the input beam at this position. This value can then again be transformed into a function by the following expression:

$$q_1 := (z) \rightarrow ABCD(q_0(L_1), L(f_1)) + z - L_1 \quad (11)$$

By this way we can define a chain of consecutive maps and in the end we can define our constraints in order to determine all missing values.

## 2.2 Entanglement

While the definition of entanglement can be described in a few sentences it is not so easy to understand what exactly entanglement is including the novel implications in theory and practice. This is mainly because the concept of entanglement violates and its consequences violate the common sense. Although quantum mechanics has proven to give correct results it does not explain why the world is as it is. Of course this is a philosophical question but to my mind it is also the reason why many people cannot realize what entanglement is. In the following sections I will try to give a short overview of the mathematics that is used and also of the applications that can arise from the control of entangled states. General information about entanglement can be found in [6] as well as in [7].

### 2.2.1 Definition

One of the basic concepts of quantum mechanics is superposition. The most general pure quantum state can be written as a superposition of all possible states. Defining a normalized orthogonal basis set allows to write the state as a weighted sum over these basis states  $\phi_i$ :

$$|\psi\rangle = \sum_i a_i |\phi_i\rangle \quad (12)$$

If we now consider a system of two particles (a bipartite system) the new basis set is created from the single particle basis by a tensor product  $|\phi_{ij}\rangle = |\phi_i\rangle_A \otimes |\phi_j\rangle_B$ , where  $A$  and  $B$  stands for the two particles. We can then allow superpositions in this product space and we see that it is possible to create states that cannot be written as a product of single particle states. All these **states which are not separable are called entangled**. As an example the state

$$|\phi_1\rangle_A \otimes |\phi_1\rangle_B \pm |\phi_2\rangle_A \otimes |\phi_2\rangle_B \quad (13)$$

is not separable. On the other hand

$$|\phi_1\rangle_A \otimes |\phi_1\rangle_B \pm |\phi_1\rangle_A \otimes |\phi_2\rangle_B = |\phi_1\rangle_A \otimes (|\phi_1\rangle \pm |\phi_2\rangle)_B \quad (14)$$

is separable and therefore not entangled.

For the more general case of mixed states one has to use density matrices  $\rho$  instead of pure states, but we have the same condition that the state is entangled if it cannot be written as  $\rho = \sum_i p_i \rho_i^A \otimes \rho_i^B$  where  $\rho_i^{A,B}$  are single photon density matrices.

### 2.2.2 The Bell states

The simplest possible and maximally entangled states are called Bell states:

$$|\Phi^\pm\rangle = \frac{1}{\sqrt{2}} (|0\rangle_A \otimes |0\rangle_B \pm |1\rangle_A \otimes |1\rangle_B) \quad (15)$$

$$|\Psi^\pm\rangle = \frac{1}{\sqrt{2}} (|0\rangle_A \otimes |1\rangle_B \pm |1\rangle_A \otimes |0\rangle_B) \quad (16)$$

If measured in the  $|0\rangle, |1\rangle$  base the  $\Phi$ -states show perfect correlation whereas the  $\Psi$ -states show anti-correlated results.

One of the states, namely the  $\Psi^-$  state is of special interest for us. It has the additional feature that it is equal independent of the base in which it is written. This means that no matter which bases we choose we will always get a perfect anti-correlation provided that we choose the same base on each side of the measurement. This is also the state that is being produced by our photon pair source which will be described below.

### 2.2.3 Some entanglement measures

The upper definition of entanglement only allows to determine whether a measured density matrix is entangled or not. But for real applications one needs to know the quality of entanglement. This is why we need entanglement measures which will be defined next. We will only mention some measures that will also be used in our measurement software in the later sections. If you are interested in an overview about the topic of entanglement measures I can recommend [9] as an easy introduction as well as [10] as a short overview.

- **von Neumann entropy:**

It is defined as

$$S(\rho) = -\text{tr}(\rho \log_2 \rho) = -\sum_i \lambda_i \log_2 \lambda_i \quad (17)$$

and describes how pure a given state is.  $\rho$  is the density matrix of the state  $\lambda_i$  are its eigenvalues. The entropy becomes a minimum of 0 for a pure state.

- **Reduced von Neumann entropy:**

In order to quantify entanglement for pure states it is important that the reduced density matrix of a pure entangled state becomes a mixed state and the extent of this mixture can be used to define the extent of entanglement. Therefor the von Neumann entropy of the reduced density matrix is also called *entropy of entanglement* and is defined as:

$$S(\psi) = -\text{tr}(\rho_A \log_2 \rho_A) = -\text{tr}(\rho_B \log_2 \rho_B) \quad (18)$$

where  $\rho_{A,B}$  are the partial traces of  $|\psi\rangle\langle\psi|$  over the subsystem A or B respectively.

- **Entanglement of formation:**

In order to handle mixed states one has to consider that the decomposition of a density matrix into a sum of pure states is not unique. Therefor the entanglement of formation has to be defined as the minimal reduced von Neumann entropy of all possible decompositions.

$$E(\rho) = \min \sum_i p_i E(\psi_i) \quad (19)$$

- **Purity:**

The purity measures the mixedness of a state  $\rho$ . It is 1 for pure states and 0 for completely mixed states and can be simply calculated as follows:

$$P(\rho) = \text{tr}(\rho^2) \quad (20)$$

See [11] for a more detailed definition.

- **Concurrence:**

As described in [12] the entanglement of formation can be analytically calculated by means of the concurrence C:

$$C(\rho) = \max \left\{ 0, \sqrt{\lambda_1} - \sqrt{\lambda_2} - \sqrt{\lambda_3} - \sqrt{\lambda_4} \right\} \quad (21)$$

where  $\lambda_i$  are the eigenvalues of the matrix  $\rho \sigma_2^A \sigma_2^B \rho^* \sigma_2^A \sigma_2^B$  and  $\lambda_1$  is the biggest one.

- **Tangle:**

This is another entanglement measure that is closely related to the concurrence, namely it can be calculated as:

$$\tau(\rho) = C(\rho)^2 \quad (22)$$

- **Fidelity:**

The fidelity simply measures the distinguishability of two states. If the states are equal it becomes 1 whereas it becomes 0 for orthogonal states. If one of the two states is a pure state it simplifies to the probability  $P_c = \langle \psi | \rho | \psi \rangle$  to measure this pure state. This is exactly the case that we need for our later quantum-state-tomography software. We have measured a density matrix  $\rho$  and we have an ideal state  $|\psi\rangle$  that we want to get. Now we can simply calculate how similar these two states are.

$$\begin{aligned} F(\rho_1, \rho_2) &= \max |\langle \psi_1 | \psi_2 \rangle|^2 \\ F(|\psi\rangle \langle \psi|, \rho) &= \langle \psi | \rho | \psi \rangle \end{aligned} \quad (23)$$

See [13] for a more detailed definition.

- **Visibility:** One problem for practical systems is that it is very complicated to measure the whole density matrix and then calculate the upper entanglement measures. This was one reason why we decided to implement an automatic quantum state tomography system that simplifies this task. Another solution that is often used in practice is to use the visibility as entanglement measure. It can simply be measured for any basis by measuring all combinations of the basis states (for the  $|H\rangle, |V\rangle$  basis these are  $|HH\rangle, |HV\rangle, |VH\rangle, |VV\rangle$ ). For a pure  $\psi^-$  state only the anti-correlated measurement should give coincidences. For the real state the difference between anti-correlated coincidences and correlated coincidences can be taken as a measure of entanglement quality. In order to normalize the measure the value has to be divided by the total number of coincidences:

$$\text{Vis}_{HV} = \frac{-C_{|HH\rangle} + C_{|HV\rangle} + C_{|VH\rangle} - C_{|VV\rangle}}{+C_{|HH\rangle} + C_{|HV\rangle} + C_{|VH\rangle} + C_{|VV\rangle}} \quad (24)$$

## 2.2.4 Applications

Since entanglement is the essential feature of photon pair source we will describe the possible applications and how they are implemented. We have to distinguish between real user applications and applications that can only be used as a part of a bigger application that is based on quantum technology:

- **Quantum Key Distribution (QKD):**

A very detailed introduction to quantum cryptography in general can be found at [14]. Quantum key distribution is the subset of quantum cryptography that handles only the secure creation of the key. Another important topic is quantum authentication.

Currently this is one of the first applications of entangled photon pairs (see [18]) that started to be used outside a pure laboratory environment. QKD is a method to create secret keys for data transmission by using the fact that a quantum state cannot be fully determined by a single measurement. As we already know our source creates photon pairs in the  $\Psi^-$  state which is independent of the measurement base that we choose provided that it is the same on both sides of the measurement.

This behaviour is now used by two parties (Alice and Bob) to create a secret key. Both parties randomly choose the measurement base for every photon. Either they measure horizontal and vertical photons or they measure  $+45^\circ$  and  $-45^\circ$  photons. So every party gets a certain bit string. In order to discard results where both parties used different bases (these would not show any correlations) they exchange the used bases via a classical communication channel. After that both parties have a perfectly anti-correlated raw key.

This procedure seems very complicated but it has an important advantage over all classical key distribution algorithms, namely the fact that it is possible to detect possible eavesdropping. This is achieved by the fact that every eavesdropper (Eve) also has to measure the state of a photon and therefore has to choose a random bases. Now there is one case where Alice and Bob choose the same bases but Eve chooses the other one. In this case the raw key that Alice and Bob create will no more be perfectly anti-correlated any longer. It can be shown that an unconditional secure key can be distilled from the raw key if the so-called qubit error rate (QBER) is below an upper-bound of about 10%.

Currently such QKD systems are limited in range as well as performance, but the big advantage is that there are security proofs that show that if such a system is used there is no possibility to crack the created code now and in the future. There is also a lot of progress in the development of quantum networks which allow end-users to exchange keys over a network of individual QKD links (see [15]). This would allow to extend the range of the key distribution and also to bypass links that are known to be insecure.

- **Quantum computers:** These are computers that work with quantum states, which makes it possible to use the quantum superposition as a powerful instrument. By applying one operation to a superposition of many input states it is possible to do the same work that would otherwise need many of operations.

Today a few first steps has been done towards the implementation of quantum algorithms but it will still be a huge task to get a version that can be used to solve real-life problems.

Nevertheless entanglement will play an important role for these computers because besides the quantum superposition this is another property that classical computers will never be able to utilize. See [8] for a detailed reference.

- **Quantum teleportation:** Teleportation means that the full quantum state of an object can be transferred to a remote object [4]. Every direct measurement would destroy the quantum state of the initial particle. The way this teleportation works is by using two ancillary entangled particles. One of the particles remains at the source and one is sent to the destination. One can now do a partial measurement in the Bell basis (a Bell measurement) of the particle that should be teleported and one of the entangled particles. This does not directly give the state of the initial particle but the state is transferred to the remote particle, but there is an additional phase, depending on the Bell measurement. The result of the Bell measurement then tells you how to recover the original phase.

This can be shown in a few lines of calculation. We start from an arbitrary state  $|S\rangle = \alpha|0\rangle + \beta|1\rangle$  that we want to teleport and an ancillary entangled pair in the  $\Psi^-$  state ( $|\Psi^-\rangle = \frac{1}{\sqrt{2}}(|01\rangle - |10\rangle)$ ). If we now write down the product state and express the first two particles by the Bell states we get the following result:

$$\begin{aligned}
 |S\rangle \otimes |\Phi^-\rangle = \frac{1}{2} \left[ & |\Psi^+\rangle \otimes (-\beta|0\rangle + \alpha|1\rangle) + \right. \\
 & |\Phi^-\rangle \otimes (+\beta|0\rangle + \alpha|1\rangle) + \\
 & |\Psi^+\rangle \otimes (-\alpha|0\rangle + \beta|1\rangle) + \\
 & \left. |\Psi^-\rangle \otimes (-\alpha|0\rangle - \beta|1\rangle) \right]
 \end{aligned}
 \tag{25}$$

In this form you directly see that depending on the Bell measurement result the remote side gets a state that is related to the initial state. Finally one only has to apply some unitary operations in order to get the original state. As a consequence of the Bell measurement the initial particle is now in one of the Bell states, which shows an important feature of quantum states, namely that it is not possible to clone a quantum state.



- **Entanglement swapping:** This topic is closely related to quantum teleportation but instead of transferring a single particle state one transfers one part of an entangled pair. So in this case we have two entangled particle pairs. We now do a Bell measurement with one particle from each pair with the result that the other two particles become entangled (see figure (3)).

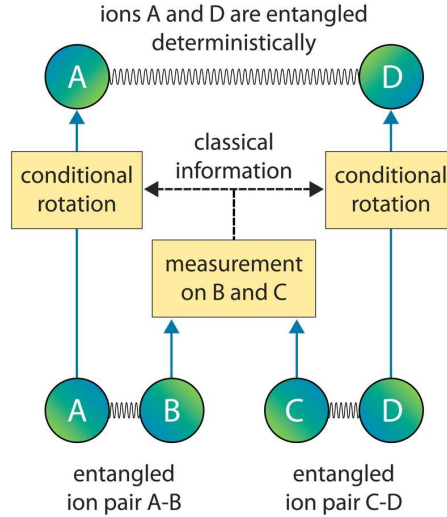


**FIGURE 3:** *Entanglement swapping. Image from University of Innsbruck*

In conjunction with quantum memory this swapping procedure allows to extend the range of a QKD system. Perhaps it would also be possible to build quantum networks in which the individual nodes need not be trusted any more. The nodes just execute the entanglement swapping procedure until the two end-users share entangled pairs. The final measurement is then done directly at the user.

- **Superdense coding:** Another interesting feature that will perhaps be used in future quantum computers is superdense coding. This procedure is based on sending qubits instead of ordinary bits from Alice to Bob. With a little trick it is possible to transmit two classical bits with only one qubit. One drawback is that both parties must share an initially entangled state, which inhibits this system to improve classical communication where no additional information is shared before the start of the transmission. But nevertheless it could be useful to speed up local communication within a quantum CPU.

I will now shortly describe how this coding scheme works. We start with a maximally entangled state that is shared by Alice and Bob, say the  $\Phi^+$  state. Alice then performs a local unitary transformation on its particle which allows her to transform the initial state into any of the four bell states. Then Alice sends her one qubit to Bob. If Bob then does a measurement in the full Bell basis he is able to determine in which state the particle is and therefore he gains two classical bits of information.

- **Quantum metrology:** This is one last application that I only want to mention shortly without a detailed description. It can be shown that using quantum effects for certain measurements can improve the precision one can reach. The maximal precision-enhancement factor is of the order of the square root of the number of measurements  $N$ . Examples for such quantum effects that can be utilized for better measurements are entanglement or squeezing.

Today we are just starting to utilize quantum effects for practical applications. But to my mind this could change very rapidly if the basic steps have been done. When the first miniaturized quantum gates and sources are available many more useful applications will turn up.

### 2.3 Spontaneous Parametric Down-Conversion

This section is about the process that we use to create entangled photon pairs. As it will be described in depth in the section [Source Design](#) our entangled photon pair source consists of a nonlinear crystal that is pumped by diode laser. Photons of this pump beam then decay into two photons. We start with the following Hamiltonian that describes the interaction of the electrical field of our pump beam  $E_p$  with the nonlinear part of the polarization  $P$  of our crystal. The linear polarization is omitted because it describes effects like aberration and dispersion which we are not interested in:

$$H = \frac{1}{2} \int_V d^3x \bar{P}^{(2)} \vec{E}_p = \frac{\epsilon_0}{2} \int_V d^3x \chi^{(2)} \vec{E}_s \vec{E}_i \vec{E}_p \quad (26)$$

Now we have to add the quantum mechanical behaviour to this equation with is done by replacing the electrical fields  $E_s$  and  $E_i$  of the signal and the idler photon by the corresponding operators. The pump beam itself can be described by a classical field because of its high intensity:

$$\begin{aligned} \vec{E}_p &= f(\vec{r}_\perp) e^{i(k_p z - \omega_p t)} \hat{e}_p \\ \vec{E}_{s/i}^\pm &= -i \sqrt{\frac{\hbar \omega_{s/i}}{2 \epsilon_0 n_{s/i} V_q}} \int d^3k_{s/i} A(\vec{k}_{s/i}) a_{\vec{k}_{s/i}}^\pm e^{-i(\vec{k}_{s/i} \vec{x} - \omega_{s/i} t)} \hat{e}_{s/i} \end{aligned} \quad (27)$$

The function  $f(\vec{r}_\perp)$  describes the radial shape of the pump beam. The polarization is given by the unit vectors  $\hat{e}_{p/s/i}$ .  $k$  and  $\omega$  denote the wavevector or the angular frequency of the photons respectively.  $A(\vec{k})$  describe the amplitude of the individual modes of the electrical field whereas  $a_{\vec{k}}^\pm$  are the corresponding operators.

Now we can directly write down the solution for the wavefunction in 1. order perturbation theory. We split the integrals into terms that we can solve later on. We also need to define the interaction time  $\tau_c$  which is the time in which the two photons interact with the pump field. This time is equal to the coherence time of the pump field:

$$\begin{aligned} |\psi\rangle &= |0\rangle - \frac{i}{\hbar} \int_0^{\tau_c} dt H(t) |0\rangle = \\ &= |0\rangle \chi_{eff}^{(2)} \int d^3k_s A(\vec{k}_s) \int d^3k_i A(\vec{k}_i) \int_0^{\tau_c} dt e^{-i(\omega_p - \omega_s - \omega_i)t} \int_V d^3x f(\vec{r}_\perp) e^{-i(\vec{k}_s + \vec{k}_i - \vec{k}_p) \vec{x}} a_{\vec{k}_s}^+ a_{\vec{k}_i}^+ |0\rangle \end{aligned} \quad (28)$$

We can solve the time integral if we assume that the coherence length of the pump field is much bigger than the length of the crystal, which means that we can let  $\tau_c$  go to infinity. Therefor we get a delta distribution which stands for the energy conservation in the down-conversion process:

$$\int_{-\infty}^{\infty} dt e^{-i(\omega_p - \omega_s - \omega_i)t} = \delta(\omega_p - \omega_s - \omega_i) \Rightarrow \boxed{\omega_p = \omega_s + \omega_i} \quad (29)$$

The spacial part is split into transversal  $(\vec{r}_\perp, \vec{k}_\perp)$  and longitudinal  $(z, k^l)$  coordinates and can be directly solved:

$$\begin{aligned} \int_V d^3x f(\vec{r}_\perp) e^{-i(\vec{k}_s + \vec{k}_i - \vec{k}_p) \vec{x}} &= \int d^2r f(\vec{r}_\perp) e^{-i(\vec{k}_s^\perp + \vec{k}_i^\perp) \vec{r}_\perp} \int_0^L dz e^{-i(k_s^l + k_i^l - k_p^l)z} = \\ &= F(k_s^\perp + k_i^\perp) \frac{e^{-i(k_s^l + k_i^l - k_p^l)L} - 1}{-i(k_s^l + k_i^l - k_p^l)} \end{aligned} \quad (30)$$

where  $F(k_s^\perp + k_i^\perp)$  is the 2 dimensional Fourier transformation of  $f(\vec{r}_\perp)$ .

With the additional assumption that the illuminated area is much bigger than the crystal the transverse distribution can be taken as constant which leads to another delta distribution  $\delta(k_s^\perp + k_i^\perp)$ . We need one final assumption to get the desired phase matching conditions, namely the fact that our crystal is very long whereby we can let the  $z$ -integration go to infinity which gives the delta distribution  $\delta(k_s^l + k_i^l - k_p^l)$ . Putting

the delta functions for the longitudinal and the transversal part together and considering that the pump beam has no transversal component gives us the following:

$$\vec{k}_p = \vec{k}_s + \vec{k}_i \quad (31)$$

Since in a birefringent crystal these  $k$  vectors are dependent on the polarization as well as the angles to the optical axis the upper phasematching conditions are only fulfilled by some certain combinations of  $k$  vectors. Here we distinguish type I and type II phasematching as described in the following subsection.

### 2.3.1 Type II

One talks about type II phasematching if one ordinary and one extra-ordinary photon is created from an extraordinary pump beam photon. Since the two created photons propagate with different velocities and therefore also different phasematching directions this leads to system of cones that are not collinear as can be seen in figure (4):

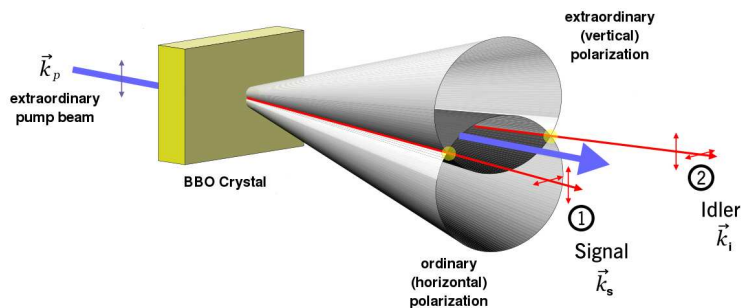


**FIGURE 4:** Schematic picture of entanglement with type II phasematching (picture from diploma work of Christian Schmid [16])

The upper case displays the case where both photons have the same energy. Thus the two cones are of the same size. Of course it is also possible that the photons have different energies which would lead to cones of different sizes. But would not lead to entanglement because the two photons would be distinguishable. Only in the symmetric case and at the cross-section of both cones we get photons where we cannot predict the individual polarization, which is a practical criterion for entanglement.

An advantage of this phasematching scenario is that the two photons get spacially separated and therefore it is possible to couple them into single-mode fibers without any additional optical element which could affect entanglement. Additionally the usage of single-mode fibers allows to select only your desired  $k$  vectors with a very high sensitivity. One problem is the the intersection of the two emission cones is not a Gaussian shaped beam which has the ratio of single and coincidence counts decreases.

### 2.3.2 Type I

In contrast to the upper case now both created photons are ordinary polarized, whereas the pump beam has extra-ordinary polarization. In this case their  $k$  vectors only depend on the created wavelength and not on its direction of propagation within the crystal. Since both photons propagate the same way in the crystal we get two emission cones that are concentric to the pump beam. Such a system is used if you want to create photons with different wavelengths because then both photons are emitted collinear and they can be split with a wavelength sensitive mirror that reflects one wavelength and transmits the other one. Another possibility is to only a small fraction of the cones and again place two detectors symmetric to the pump beam, which directly leads to a spacial separation of the photons.

### 2.3.3 Optimal Coupling

Now we want to calculate our optimal coupling system as described in [17]. At first we assume that our pump beam is a plain wave and the beam characteristics of the created photon pairs is only depending on the dispersion within the BBO crystal. We use the dependence of the dispersion on the actual wavelength which can be calculated numerically. In our case for  $810nm$  we get  $\frac{d\Phi}{d\lambda} = 0.045 \frac{\circ}{nm}$ . With a desired bandwidth of  $\Delta\lambda = 5nm$  this gives us the following divergence angle which in turn gives the needed beam waist:

$$\begin{aligned} \Delta\Phi &= \frac{d\Phi}{d\lambda} \Delta\lambda = 0.225^\circ \\ \omega_0 &= M \frac{\lambda}{\pi \Delta\Phi} = 65.66 \mu m |_{M=1} \end{aligned} \tag{32}$$

Since we cannot calculate the final beam quality which is described by the  $M$  parameter our result only gives us the order of magnitude and not an exact value. The bandwidth and divergence angle of the pump beam will also have an influence on the created photon pairs and the calculation would become more complex. But in any case you will get the following relation. The bigger the bandwidth that you accept the more photons you will collect but the worse is the quality of entanglement that you will experience. It is only a matter of the application what you prefer.

Now that we have selected the beam profile of our created photons this allows us to calculate the optimal pump beam waist. This is done by the simple geometrical consideration that the overlap of the created beams with the pump beam should be optimal. In practice this can be archived by choosing the pump beam waist  $\omega_p = \omega_0$ . Since the emission cones are tilted a few degrees against the pump beam axis the waist is a bit too large but this should again only give the correct order of magnitude.

### 2.3.4 Walkoff Compensation

There are also some unwanted effects of the down conversion process that we did not mention yet. Namely there are two so called walkoff effects that theoretically allow to distinguish the two created photons which leads to a worse entanglement visibility. I will now describe both of these effects and finally show a way how to compensated them:

First we will deal with the longitudinal walkoff (see figure (5)). The term longitudinal means that there is an offset in the direction of propagation between the two photons. Since one photon is ordinary polarized whereas the other is extra-ordinary polarized they propagate with different velocities within the crystal and thus become distinguishable.

The second effect if called transversal walkoff (see figure (6)) and it means that since we use extraordinary beams we get deflections although the input beam is orthogonal to the crystal surface. At first the extraordinary pump beam itself gets deflected. On this deflected path photon pairs are created. One of these photons is then also deflected like the pump beam. Therefor the shape of the created extraordinary beam after the BBO crystal remains circular. In contrast to this the ordinary photons propagate parallel to the pump beam from the location where they are created. Thus they lead to an elliptical output beam after the BBO.

Although both of these effects are irreversible there is a method to correct them at least in average. The main problem of this correction is that you do not know the place where the photons are created within the crystal. So the effective length of the BBO crystal changes from 0 to the full crystal length depending on the actual place of the pair creation.

When we now want to create a system that partly corrects both of these offset effects one part that we definitely need is an additional crystal with the same optical properties as the original one. Since the average place of pair creation is in the middle of the BBO crystal we take a second BBO of the half length for this purpose. A simple system that correct the longitudinal walkoff would be to place this second BBO after the original one but rotate it by  $90^\circ$ . Due to this the fast axis of the first BBO follows the slow axis of the second and vice versa. In average both effects compensate, but the drawback is that the transversal walkoff is not compensated at all. On the other hand the second BBO could be rotated by  $180^\circ$  which would simply

invert the direction of deflection of the extraordinary photon. But then the longitudinal walkoff gets worse. So what we are looking for is a system that combines both of these corrections.

The way this is done is by simply replacing the ordinary with the extraordinary photon by a half-waveplate. This waveplate rotates the polarization by  $90^\circ$  which transforms the original ordinary photon into an extraordinary one and vica versa. As before we then use a second BBO, but now in the same orientation as the original one. Since both photons exchanged their polarizations the one that was slower in the first BBO is then faster and the other way round, which compensates the longitudinal walkoff.

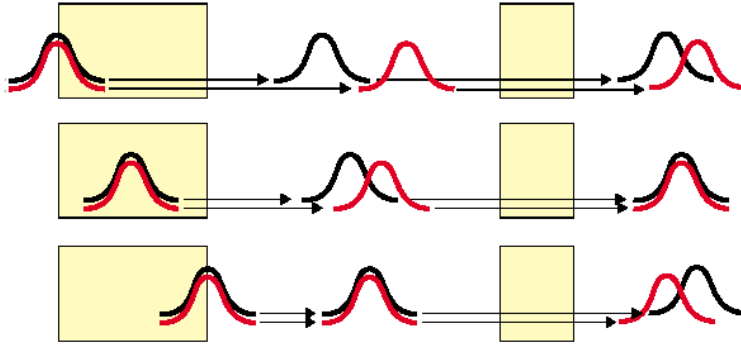


**FIGURE 5:** *Longitudinal walkoff effect and its compensation*

The transversal walkoff is also mitigated because the photon that directly passed the first BBO is now deflected and so the centers of the two beams match again, as can be seen in the following graphic:

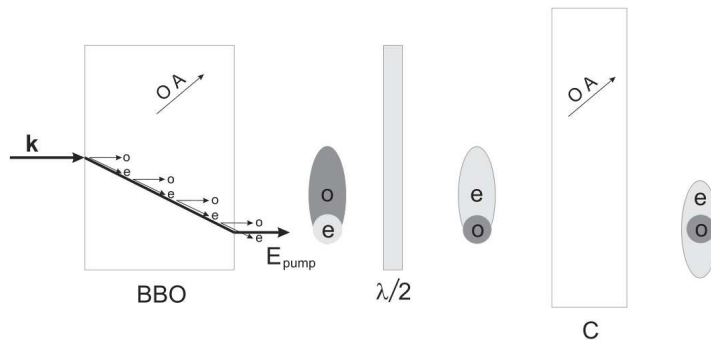


**FIGURE 6:** *Transversal walkoff effect and its compensation*

## 2.4 The Poincare sphere

For our final measurement system that does a full quantum state tomography we need to handle polarization states of a 2-qubit-system. For a better understanding we will start with the measurement of single qubits in this section. First we start with a general density matrix of a single qubit state, which can be written as:

$$\hat{\rho} = \sum_i p_i |\psi_i\rangle\langle\psi_i| \quad \sum_i p_i = 1 \quad (33)$$

We see that the general density matrix contains a sum over infinitely many states, but due to the fact that we only have a certain number of degrees of freedom, this infinite sum can always be reduced to a sum over two orthogonal eigenstates by simply diagonalizing the density matrix. This is possible because the density matrix is a Hermitian matrix.

If you take the hermeticity and that the trace of the matrix must be 1 this leads to 3 independent parameters that are available to describe all allowed density matrices. One possible parametrization of this

general density matrix are the so-called Stokes parameters  $S_i$  combined with the three Pauli matrices and the unit matrix:

$$\hat{\rho} = \frac{1}{2} \sum_i S_i \hat{\sigma}_i \quad S_i = \text{Tr} \{ \hat{\sigma}_i \hat{\rho} \} \quad (34)$$

$$\hat{\sigma}_0 = \begin{pmatrix} 1 & 0 \\ 0 & 1 \end{pmatrix} \quad \hat{\sigma}_1 = \begin{pmatrix} 0 & 1 \\ 1 & 0 \end{pmatrix} \quad \hat{\sigma}_2 = \begin{pmatrix} 0 & -i \\ i & 0 \end{pmatrix} \quad \hat{\sigma}_3 = \begin{pmatrix} 1 & 0 \\ 0 & -1 \end{pmatrix} \quad (35)$$

In order to understand the meaning of the Stokes parameters one can rewrite the Pauli operators  $\hat{\sigma}_i$  as a sum of two projection operators  $\hat{P}_i$ . This shows that the Stokes parameter  $S_i$  itself can also be written as sum of two polarization probabilities  $P_i$ :

$$\hat{\sigma}_0 = \hat{P}_{|H\rangle} + \hat{P}_{|V\rangle} \quad \Leftrightarrow \quad S_0 = P_{|H\rangle} + P_{|V\rangle} \quad (36)$$

$$\hat{\sigma}_1 = \hat{P}_{|D\rangle} - \hat{P}_{|A\rangle} \quad \Leftrightarrow \quad S_1 = P_{|D\rangle} - P_{|A\rangle} \quad (37)$$

$$\hat{\sigma}_2 = \hat{P}_{|R\rangle} - \hat{P}_{|L\rangle} \quad \Leftrightarrow \quad S_2 = P_{|R\rangle} - P_{|L\rangle} \quad (38)$$

$$\hat{\sigma}_3 = \hat{P}_{|H\rangle} - \hat{P}_{|V\rangle} \quad \Leftrightarrow \quad S_3 = P_{|H\rangle} - P_{|V\rangle} \quad (39)$$

The basis that is used in the upper case is called the canonical basis and it consists of horizontal  $H$ , vertical  $V$ , diagonal  $D$ , anti-diagonal  $A$ , right-circular  $R$ , and left-circular  $L$  polarization.

Since the trace of the density matrix always has to be 1 the  $S_0$  parameter is also always 1. In the classical view this parameter describes the total intensity of the beam which is also independent of its polarization state. Therefore now we have three independent real variables that allow us to specify any possible polarization state for unpolarized, partially polarized or fully polarized light. If we draw these three parameters in a 3D diagram we see that all allowed states fall into a sphere of radius 1 which is shown in figure (7). The center of the sphere is the totally unpolarized state where all projective measurement give the same result and thus all  $S_i = 0$  for  $i = 1, 2, 3$ . Partially polarized light lies within the sphere whereas totally polarized states lie on its surface.

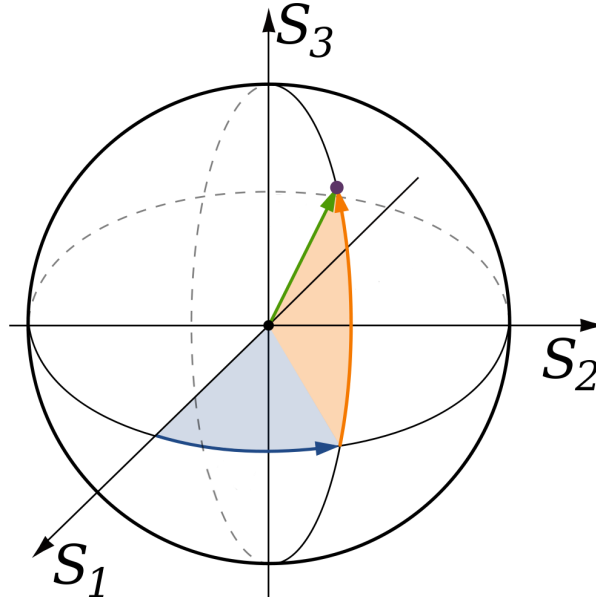


**FIGURE 7:** Poincare sphere with an example polarization vector. According to there definition the  $S_1, S_2, S_3$  axes can be mapped to the  $|D\rangle, |R\rangle, |H\rangle$  states

One big advantage of this representation is that one can visualize the action of any unitary operation by a rotation about a certain axis. For example a half / quarter waveplate leads to a  $180^\circ$  /  $90^\circ$  rotation about an axis that passes through the equator. The angle between the axis and the state in the Poincare sphere is two times the angle between optical axis and the polarization direction. For example a half waveplate at a real world angle of  $45^\circ$  leads to a rotation about an axis that stands orthogonal to the initial state. If we now rotate our state by  $180^\circ$  about these axes we get a state that is on the opposite side of the Poincare sphere.

The Poincare sphere is introduced for better understanding of the action of combinations of optical elements changing polarization. As an example I can mention that we implemented a measurement system consisting of one half and one quarter waveplate. But in addition of the desired effects of these waveplates we also got an arbitrary polarization rotation by our single mode fiber. First we tried to compensate the influence of the fiber directly with our measurement system, but we found out very quickly that this is not so simple. If for example we want to transform a  $|H\rangle$  state into a  $|V\rangle$  state this can simply be done by a half waveplate at  $45^\circ$ . But if now the fiber rotates the initial  $|H\rangle$  state this would also need a correction of the waveplate settings. Although this problem can be solved theoretically in practice it would be more useful to add additional waveplates or fiber based polarization controllers to the system.

At the close of this section we can summarize that a consecutive projection measurement in three linearly independent bases (as well as the full intensity) allows to define our Stokes parameters and thus our full single qubit state.

## 2.5 Quantum state tomography

This section is only a generalization of the single qubit measurement described in the upper section [The Poincare sphere](#). A very good introductory manuscript can be found at [19]. In our case we want to measure the state of an entangled photon pair, a 2-qubit-state. Doing a  $n$ -qubit measurement would not change the procedure but only the effort that is needed.

As before we can disassemble our density matrix into a basis of Pauli matrices:

$$\hat{\rho} = \frac{1}{2^n} \sum_{i_1, i_2, \dots, i_n=0}^3 S_{i_1, i_2, \dots, i_n} \hat{\sigma}_{i_1} \otimes \hat{\sigma}_{i_2} \otimes \dots \otimes \hat{\sigma}_{i_n} \quad (40)$$

For case of normalization  $S_{0,0,\dots,0} = 1$ , which leaves  $4^n - 1$  parameters for a full description of the quantum state. As before we can decompose our products of Pauli matrices into a number of projection operators and thus express our Stokes parameters by these measurable projections.

### 2.5.1 Maximum likelihood technique

One practical problem that we are facing is that the density matrix that is reconstructed must be Hermitian in order to represent a physical quantum state. In theory this is achieved by decomposing the matrix into a sum of Pauli matrices which are themselves Hermitian. And as already mentioned these Pauli matrices are then further decomposed into two projection operators. In theory this procedure will lead to a uniquely defined Hermitian density matrix, but in practice there is the problem that the two projective measurements are not exactly equal. Each measurement system has a certain efficiency and thus the weight of the two measurements will not be the same and will therefore not result in a Hermitian density matrix.

Using this directly reconstructed matrix will lead to many problems for further calculations. The solution for the problem is called maximum likelihood technique. First one calculates the state directly and then looks for Hermitian matrices that almost look like this state. This is achieved by minimizing a likelihood function using a numerical algorithm. This leads to the fact the final result depends on the used likelihood function as well as on the numerical algorithm and is not unique any longer.

Since we want to use a numerical optimization the parametrization of the density matrix using Pauli matrices is not convenient, because this would require an additional constraint for the Stokes parameters that

are allowed. We want to create a non-negative definite Hermitian matrix of trace 1, which we get from the following equation:

$$\hat{\rho} = \frac{\hat{T}^\dagger \hat{T}}{\text{tr}(\hat{T}^\dagger \hat{T})} \quad \hat{T}(\vec{t}) = \begin{pmatrix} t_1 & 0 & \dots & 0 \\ t_{2^{n+1}} + it_{2^{n+2}} & t_2 & \dots & 0 \\ \dots & \dots & \dots & 0 \\ t_{4^{n-1}} + it_{4^n} & t_{4^{n-3}} + it_{4^{n-2}} & t_{4^{n-5}} + it_{4^{n-4}} & t_{2^n} \end{pmatrix} \quad (41)$$

where we decided to use tri-diagonal form of the matrix  $\hat{T}$ . Due to the fact that the trace in the denominator guarantees the normalization all parameters  $t$  can be arbitrarily chosen.

The last component that we need for our calculation is the likelihood function, which gives us the probability that a given density matrix will reconstruct the measured count rates. Unfortunately this function depends on the measurement system, especially on the statistical distribution of the counts. Therefore we need to assume a Gaussian counting statistics for the further calculation.

The expected count rate for the  $\nu^{\text{th}}$  measurement on the  $r^{\text{th}}$  detector can be written as (see [19])

$$\bar{n}_{\nu,r} = I_\nu E_r \text{tr} \left\{ |\psi_{\nu,r}\rangle \langle \psi_{\nu,r}| \hat{T}(\vec{t}) \hat{T}^\dagger(\vec{t}) \right\} + n_{\nu,r}^{\text{accid}} \quad (42)$$

where the trace gives the probability to measure a certain state  $|\psi_{\nu,r}\rangle$ . This probability has to be multiplied with the total intensity of the corresponding measurement  $I_\nu$  as well as with the efficiency of the used detector  $E_r$ . Additionally one can consider accidental coincidences.

With this expression for the expected individual count rates as well as a Gaussian counting statistics we get the following total probability that our density matrix yields the measured rates:

$$P \propto \prod_{\nu,r} \exp \left[ -\frac{(\bar{n}_{\nu,r} - n_{\nu,r})^2}{2\sigma_{\nu,r}^2} \right] \quad \sigma_{\nu,r} \approx \sqrt{\bar{n}_{\nu,r}} \quad (43)$$

This probability now needs to be maximized to find the ideal density matrix for our measured count rates. In practice it is easier to maximize the logarithm of the function whereby the product is transformed into a sum over the individual measurements. Instead of searching for a maximum most available algorithms perform a minimization. This is why we use the negation of the logarithm and finally get the following expression as our likelihood function:

$$\mathcal{L}(\vec{t}) = \sum_{\nu,r} \frac{(\bar{n}_{\nu,r} - n_{\nu,r})^2}{2\bar{n}_{\nu,r}} \quad (44)$$

The last step is to use a numerical optimization algorithm to find the optimal  $t_i$  values and then calculate the corresponding density matrix.

### 2.5.2 Systematic errors

In practical systems we can identify some sources of systematic errors. Some of them can be quantified and are easy to eliminate. Examples for such errors are varying total intensities, different detector efficiencies or the beam splitter crosstalk if using two detectors per side. In order to correct these errors we have to realize the reason for the error and then do some measurements that allow to estimate the amount of the error only by means of available data. For example one can measure the beam splitter crosstalk using classical light and then correct the estimated count rates (42) accordingly. The only difficulty that occurs is that the measurement accuracy is limited and thus the error cannot be compensated perfectly.

Another class of errors exists which cannot be quantified by some easy measurements. Because it would need too much additional effort to measure all influences that would be required for a complete model, one can use a simplified model instead. This will only lead to a partial correction, but therefore it will be easier to implement.



One additional degree of freedom that one has are local operations and classical communication (LOCC). This idea is closely related to the entanglement measures defined above. Since entanglement is a collective feature these measures should not increase when applying only local quantum operation to the system. Classical communication cannot improve the entanglement as well. For our purpose of the characterization of an entangled photon source we would like to get an at most pure maximally entangled state. We can thus apply some arbitrary LOCC to reconstructed density matrix and do a further optimization to determine the parameters of the LOCC. In this way some errors that cannot be quantified can also be corrected.

An example for such an error is the polarization rotation caused by the deflection of the used glass fibers. One way to correct this error would be to measure the influence of the fiber using classical light and a polarimeter and then correct it by means of the polarization controller or mathematically in the analysis software. Due to the fact that the behaviour of the fiber changes over time and especially if the fiber is moved this measurement has to be done in situ, which means a notable additional effort. The other way of solving this problem is to reconstruct the density matrix without consideration of the polarization rotation and then allow for local unitary operations such that the overlap of the rotated density with the ideal one becomes a maximum.

### 2.5.3 Number of detectors to use

One can show that for a full characterization of the density matrix one needs  $4^n$  projective measurements, when using  $4n$  detectors, which means 1 detector per side. In order to reduce the overall measurement time one can use polarizing beam splitter and measure two orthogonal bases at the same time. This way one can reduce the number of consecutive measurements to  $3^n$ . Additionally the usage of both complimentary orthogonal measurements allows to easily transform the measured counts into probabilities and thus also improves the accuracy of the measurement. If one only takes the pure measurement time into account the usage of a complete bases would also be preferable for the measurement with 1 detector per side. This would result in 36 measurements for a 2 qubit system instead of 16, but if you sum up the total time needed in order to reach a certain accuracy it would be faster. In practice one also has to consider the time needed to re-position the waveplates between the individual measurements. Only for very slow systems the measurement in an incomplete bases would pay off.

Also the number of counts that are necessary in order to reach a certain accuracy is very interesting. Monte-carlo simulations have been used to simulated the behaviour of the state tomography for different quantum states. An example for such a calculation can be found at [19]. Typical values to reach a theoretical fidelity of more than 99% are a few thousand counts per measurement.



### 3 Source Design

The following schematic diagram shows all important components of the entangled photon source which will be described in depth in the following subsections. The main part of the source is a nonlinear crystal in which our entangled photon pairs are created. Therefore we use a 405nm pump-beam that is of extra-ordinary polarization. We use a crystal that is cut to fulfill type II phasematching conditions, which means that the two created photons are of orthogonal polarization and we get one ordinary and one extraordinary photon. We want to build a symmetric system where both photons have the same energy which leads to a doubled wavelength of 810nm for our pair photons. Our entangled photons are then only created at the cross-sections of the two emission cones for ordinary and extraordinary photons. This leads to certain  $k$  vectors that we will then select by the usage of single-mode fibers which provide a very narrow acceptance angle.

I tried to split the whole source into the following functional blocks. First we have a diode laser with a low coherence length but a high output power. The beam is then focused by a focusing optic on a BBO crystal where the entangled photon pairs are created. For better results there also has to be a walkoff compensation. Finally the photons are collected into a single mode fiber by a corresponding coupling optic. In order to guarantee stable operation a 4-quadrant-photodiode continuously checks the beam position and it can be corrected if necessary.

The necessary theoretical background for all of these blocks is provided in the theoretical part at the beginning of this work (see [Theory](#)).

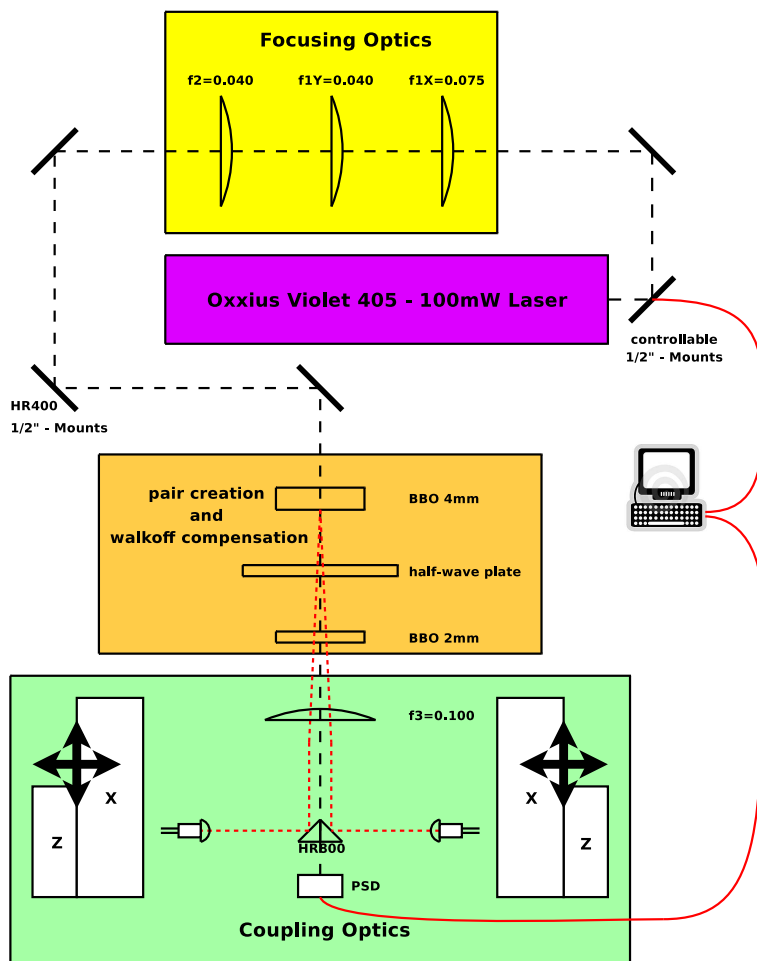


FIGURE 8: Toplevel design of our entangled photon source.

### 3.1 Laser Violet-405 from Oxxius

In contrast to former EPR sources we use an inexpensive diode-laser with a relatively low coherence length (see figure (9)). We would expect a worse visibility, but due to the fact that you get lasers with a higher output power for the same price we hope to get a better cost effectiveness. Smaller size and easier handling are also some advantages of our laser. For later systems one could use a bare laserdiode and implement temperature and current control loops as part of the integrated source electronics. At the moment we decided to use pre-built diode module which saves us the trouble with the details of the diode control.

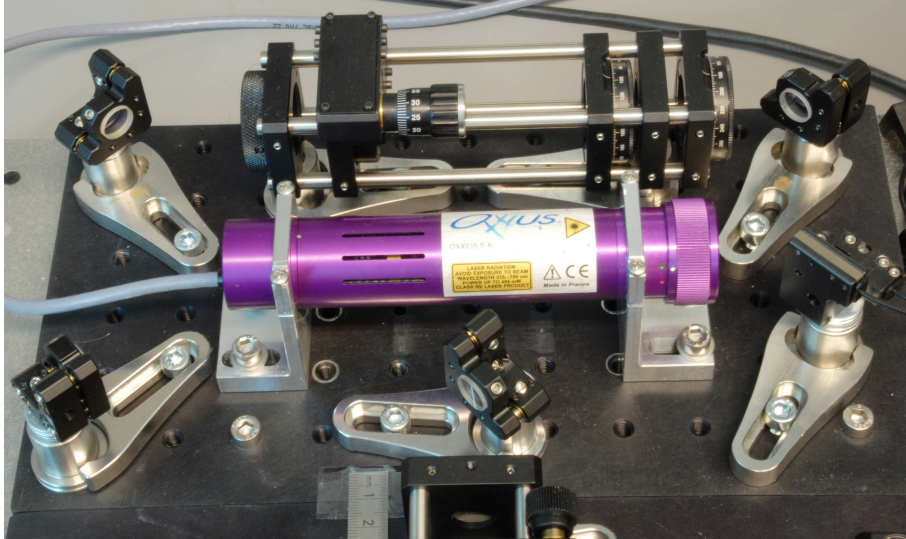


FIGURE 9: *Laser with focusing optics and beam control*

#### 3.1.1 Measurement of the power control feature

The Violet-405 Laser allows to control the laser beam output power by an external voltage from 0-5VDC on the ANALOG input. Additionally you have to apply +5VDC on the TTL input and switch to "MOD" operation. In order to avoid the need for some additional power supplies I built a small voltage divider that allows to control the voltage from 0-5VDC. Measuring the applied voltage as well as the output power gives the following result (see figure (10)):

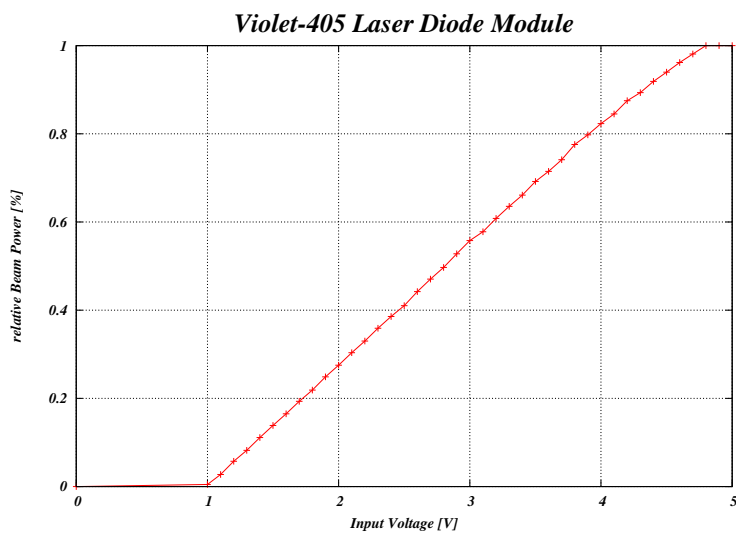


FIGURE 10: *Laser power control characteristics*

### 3.1.2 Measurement of the laser spectrum

In our final system with the new laser we experienced the problem that the wavelength of our unstabilized laser diode does not match to the narrow-band filters that we used. Additionally we found out that the spectrum of the laser diode module also depends on its output power. The variation is only about 1nm in wavelength but since this light is down-converted this value has to be doubled and we use 4nm filters in our measurement system. This means that if the center wavelength of the pump beam is shifted by 1 nm the created photon spectrum will be shifted onto the boundary of the pass band.

Figure (11) shows measured spectra of the old as well as the new laser source. One can see that the center wavelength of the new laser is shifted compared with the original laser if operating in power control mode.

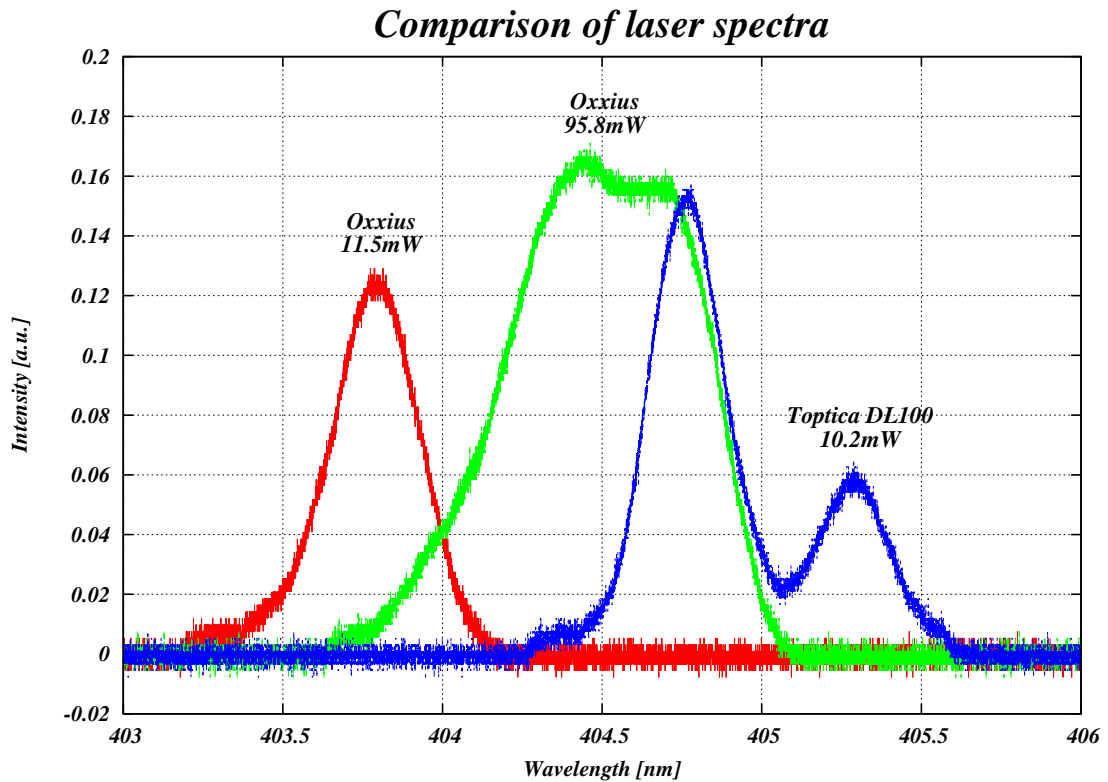
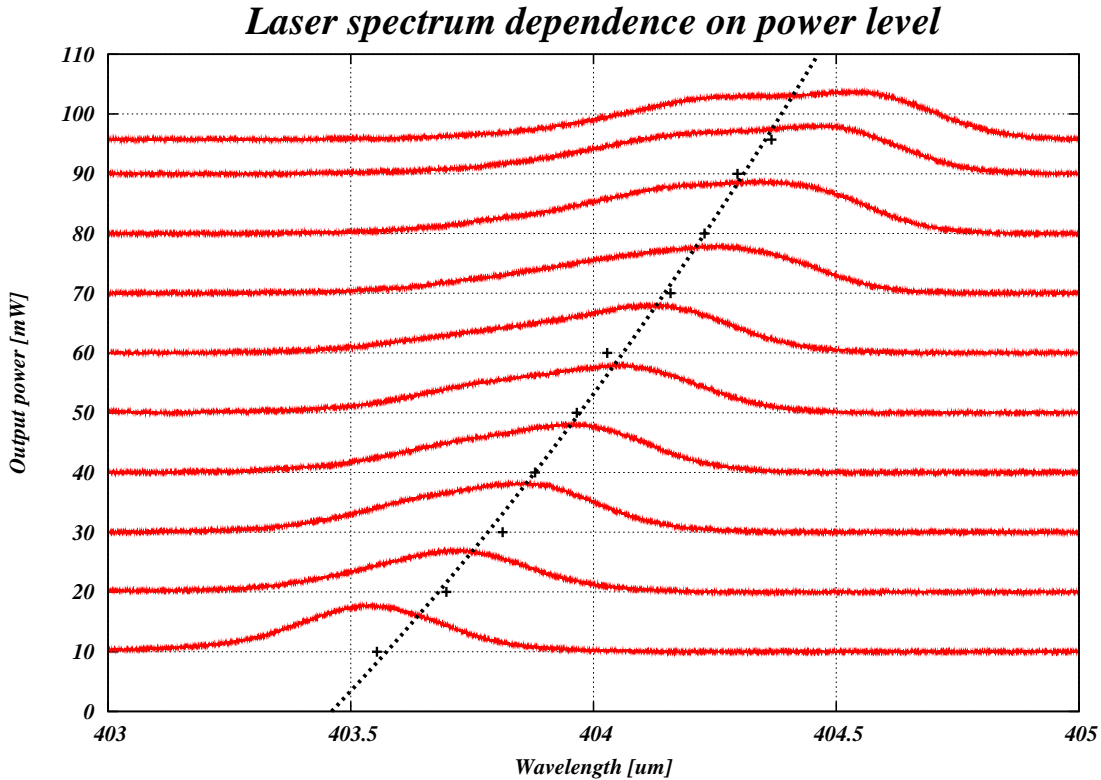


FIGURE 11: Comparison of laser wavelengths that shows a significant shift when the new laser is used in power control mode.

In order to get a full characterization of our laser we additionally measured a series of spectra with different power control settings. We started from zero with steps of 10mW up to the full power of the laser which was 95.7mW. The number on the Y-axis of the diagram show that power setting of the corresponding spectrum (see figure (12)):



**FIGURE 12:** *Laser spectrum dependence on power level: These graphs show that the more the power is down-regulated the bigger is the offset of the mean wavelength. Additionally we can see that for high power the bandwidth of the laser gets significantly larger. The individual spectra belong to power levels that can be read from the corresponding value on the y axis. The black (dotted) line shows the laser power over the center of weight of the spectra.*

### 3.1.3 Measurement of the beam profile

In order to get the parameters of our input beam we used a CCD camera LBA-USB 620U from Spiricon Laser Beam Diagnostics and plotted the beam waist of major and minor axes over the distance. We used the major/minor axes in order to avoid errors due to a slightly rotated beam. After the measurement we mapped the results to the real X/Y axes. To process our data we used some Linux commandline tools like `sed`, `awk`, `gnuplot`. I also tried to write an overall Maple worksheet that combines all calculations concerning the focusing lens system, but for certain input data I had problems creating a proper fitting curve. Using this simple `gnuplot` script always worked for my data. It simply plots the measured data points and tries to fit a curve according to equation (2):

```
# least squares fit for M2-gaussian-beam
w1(z) = sqrt(M1**2*405e-9/3.1415 * z0_1 * (1+((z-d1)**2)/(z0_1**2)));
w2(z) = sqrt(M2**2*405e-9/3.1415 * z0_2 * (1+((z-d2)**2)/(z0_2**2)));
fit w1(x) 'results' using ($1):($16*1e-6) via z0_1,d1,M1;
fit w2(x) 'results' using ($1):($21*1e-6) via z0_2,d2,M2;
print 'Major: M=', M1, ', d=', d1, ', z0=', z0_1
print 'Minor: M=', M2, ', d=', d2, ', z0=', z0_2
```

```

# output measured data plus fitted curve
set grid
plot 'results' using ($1):($16*1e-6) w lp 1, \
'results' using ($1):($21*1e-6) w lp 2, \
w1(x) w l 3, \
w2(x) w l 4

```

For our Violet-405 laser diode module from Oxixus which has a measured output power of 100mW we got the results shown in figure (13) (distances measured from laser head):

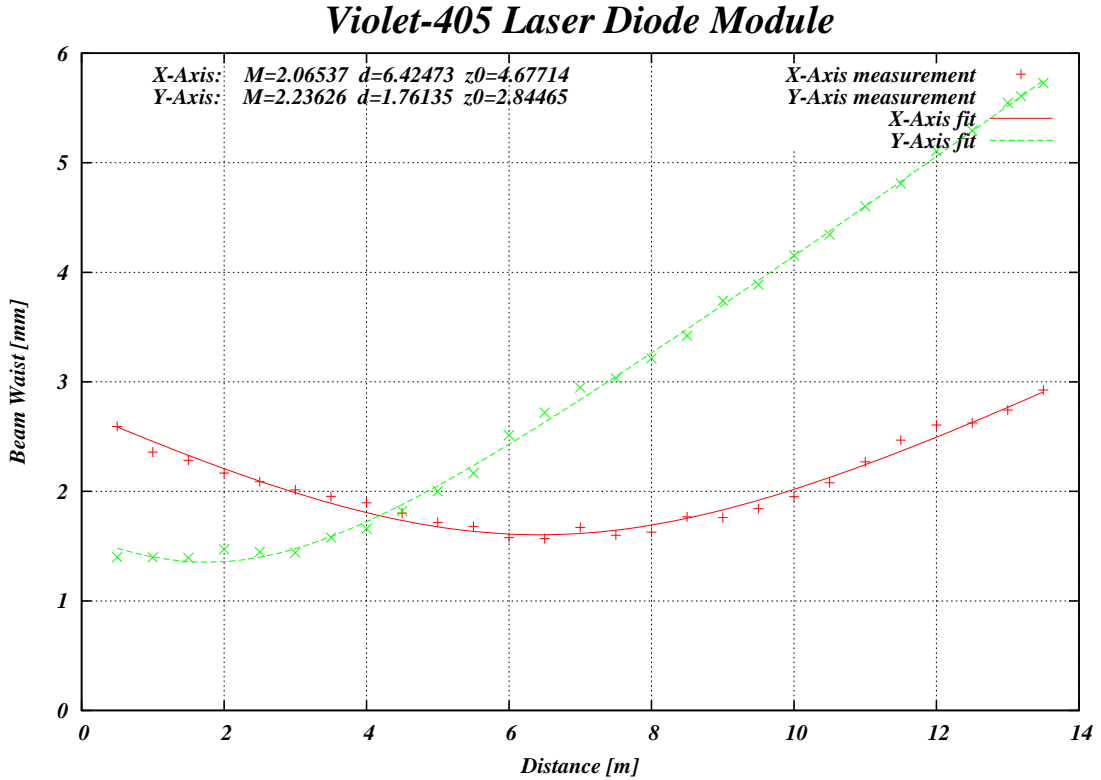


**FIGURE 13:** Laser beam characteristics of the Oxixus laser diode module. It shows an astigmatism as well as an ellipticity which has to be compensated in order to obtain a maximal intensity in the focus.

## 3.2 Focusing Optics

This section describes how the focusing optics for our source was designed. The first step is to find out with pump beam you currently have and how it should look like in order to yield optimal pair creation. This process was already described in [17], but I will try to give a more practical view on this topic. The second step will be to calculate a lens system that transforms the laser beam into the needed beam.

This process also gives you the possibility to introduce a clear interface between focusing optics and the rest of the source. So it will be possible to build a modular system where you can simply switch to a more powerful laser if you need higher pair rates without touching the rest of the system.

### 3.2.1 Theoretical considerations

The next step is to find some criteria that allow us to completely determine our beam profile. Since the focusing optics is the first part of the whole EPR source one could think that you can choose the beam as you like if the rest of the system is then matched to this choice. But according to [17] the input beam can be approximated as a plain wave because the wave front of a Gaussian beam within the Rayleigh range looks

nearly like that of a plane wave. So as we have seen in section [Optimal Coupling](#) the optimal focus waist depends approximately only on the dispersion within the nonlinear crystal. But due to the fact that we still can adjust the beam waist in a certain range we used a waist of  $100\mu m$  as a first reference value, the same value as measured from the "Bank Source" (see [\[18\]](#), [\[2\]](#)).

In order to calculate our lens system we approximate our input beam as Gaussian beam. Since we have no ideal beam we get a certain  $M^2$  value [\(4\)](#) bigger than 1. In our simulations we only use this  $M^2$  value to fit calculated data to measurement results. It makes no sense to calculate the  $M^2$  value within the simulation because you have no control about this parameter in practice. Many design decisions can be made by reason of earlier experiences. For example we knew that the focusing system can be made smaller by using two lenses for focusing instead of one (this is also shown as a simple MAPLE calculation at [Example calculation with MAPLE](#)). Another thing we could say in advance is that the laser beam ellipticity should be corrected. Thus we need at least one cylindrical lens in the setup.

After some initial calculations of some different lens arrangements it proved useful to use two cylindrical lenses to correct beam ellipticity as well as the astigmatism and focus to a very small focus first (in our case about  $10\mu m$ ). The last lens is then a spherical one that expands the beam again and allows to vary beam size by changing lens position. So basically we have a focusing system that allows us to change all needed parameters in a certain range by adjustment screws. This is very important because due to practical imperfections the calculated beam does not exactly match the physical one.

### 3.2.2 Simulation

With this input data we can now simulate how a beam is transformed by our lens system using the ABCD matrix formalism. In order to derive the lens system we decided to use the symbolical simulation tool MAPLE to do our calculations. At first we defined our input beam as well as the transformation equations for all three lenses of the focusing system. Variables are used for still unknown lens positions as well as focal lengths. One difficulty that you have to solve is how to reduce your degrees of freedom in order to find enough criteria to define the lens system. In our case we decided to fix the focal lengths of the lenses if possible and only use the lens positions as real variables. This is also useful because there are only limited focal lengths available.

So the first equation that we used to define our lens system followed from the requirement that focus positions in X and Y direction should coincide. We can now fix the first lens position as well as the focal lengths of the cylindrical lenses and calculate the position of the second lens. But since we only have one degree of freedom here (the second lens' position) it is not possible to match the beam waist. But trying out different combinations of focal lengths allowed to select the best possible choice. In theory it is also possible to perfectly match beam waists by moving both cylindrical lens positions relative to the laser source, but in practice it did not improve the situation.

Now that we already have an intermediate focus we only need to fix the position and focal length of the spherical lens at the end of the system. In principle it is possible to use any lens here. Using a small focal length increases lens aberration while a bigger focal length increases the overall size of the system. By adjusting the position of the lens you can still change the focus waist but this of course also changes the focus position.

### 3.2.3 Practical considerations

Now that we have calculated our "perfect" lens system we have to think about practical realization. The first thing that could be fixed are the lenses. We used lenses of BK7 glass and with anti-reflection coating (fused silica lenses would be better for 405nm wavelength, but unfortunately they were not available). For the cylindrical lenses we decided to use a round substrate in order to mount all lenses into default lens holders. For the spherical lens we decided to try out some alternatives namely plano-convex, best-form as well as an achromatic lens. Best-form and achromatic lens should improve beam quality but in later tests we found out that the simple plano-convex lens performs best with our coupling system.

We decided to mount our lenses in a cage system which offers high stability and all needed degrees of



freedom to adjust the lenses. Cylindrical lenses are mounted in rotation mounts. Translation in z-direction is done via a z-translation-stage that is temporarily mounted next to the rotation mount. After adjustment it is removed again. The spherical lens is mounted in another z-translation-stage in order to offer a variable beam waist for later optimization.

Another thing that had to be considered is the beam drift due to temperature fluctuations and other effects. In order to compensate this we added an active closed loop control. See section [Beam Control Loop](#) for a detailed description of the controlled system. Therefor we added some mirrors right after the laser in order to control beam position. One or two of these mirrors can then me mounted on some controllable mirror mounts in order to implement the controlling element. On the other hand we need a position sensitive device (PSD) anywhere in the system.

### 3.2.4 The Result

The calculation leads to the results shown in table (2):

Name	Lens type	focal length	position (relative to laser)
L1X	cylindrical	75mm	100.00mm
L1Y	cylindrical	40mm	134.67mm
L2	spherical	40mm	—

TABLE 2: *Calculated lens system*

The position of the L2 lens decides which beam waist we get and where the focus is located. This position must be adjusted in the final setup using the CCD camera because it has a very strong effect on the final beam characteristics. The following graphs show the theoretical dependence of beam waist and location on the lens position:

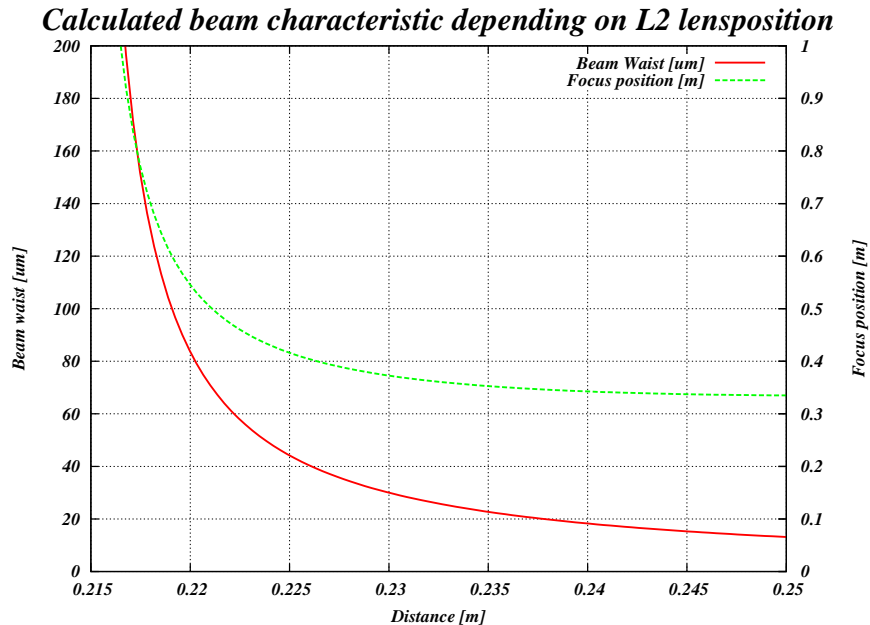
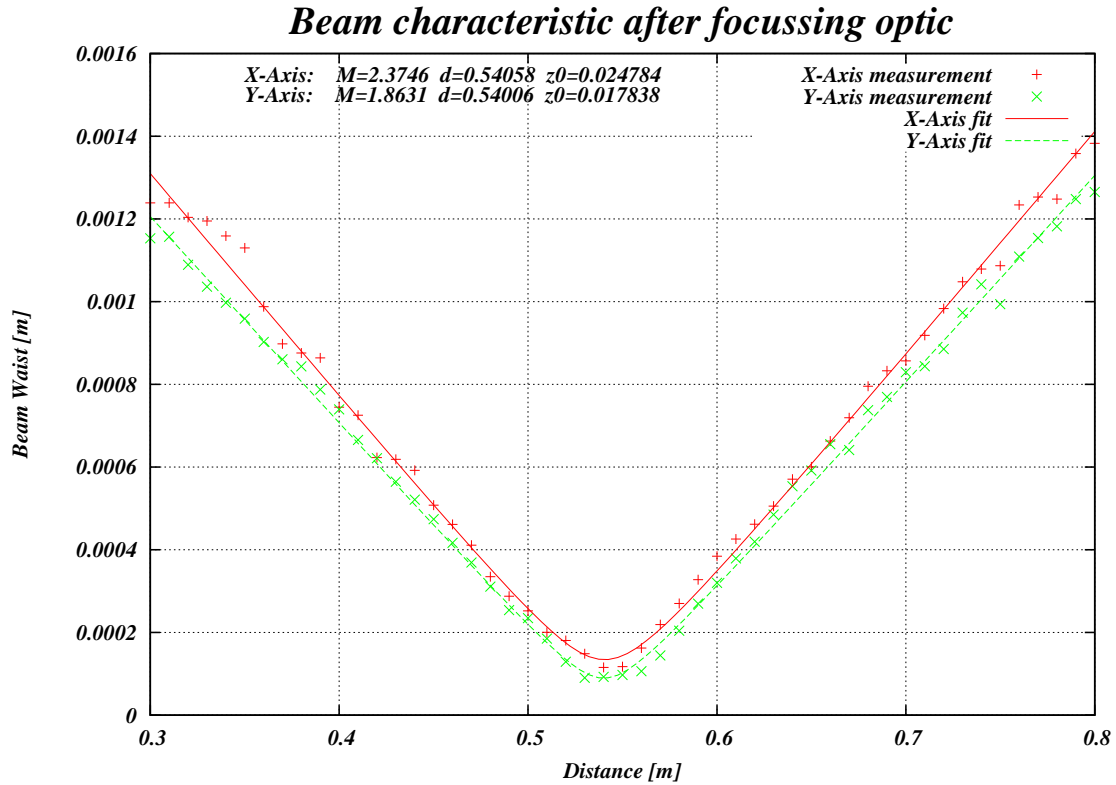


FIGURE 14: *Beam waist  $w_2$  and focus location  $d_2$  and over L2 lens position. This diagram shows that we can select arbitrary beam waist up to about  $150\mu\text{m}$ . The upper limit is only given by the maximal system size, since with bigger beam waists the focus distance would increase rapidly.*

After some adjustment we measured the following results:



**FIGURE 15:** Laser beam characteristics after focusing optics. If you compare this with the input beam in figure (13) you can see that the astigmatism is perfectly corrected and also the ellipticity is very small.

One can see that the focus position of X and Y axis are almost the same while the beam waist varies from about  $130 \mu\text{m}$  of the X-axis to about  $90 \mu\text{m}$  of the Y-axis. Off-the-shelf lenses would help to match also the beam diameter in both axes.

Finally we can say that we have a very stable focusing system, that allows us to vary the beam waist that we want to have. Additionally the beam profile looks very much like a Gaussian beam, and much better than the beam of the old grating stabilized laser source. But we have to be aware of the broader spectrum of the new laser source.

### 3.2.5 Comparison with the original laser system

In order to check how good our laser system works we exchanged the laser of the original source and compared the created pair rates (see table (3)). We added a neutral density filter to get nearly the same power in both systems. We measured the coincidence rate as well as the visibility in the  $0^\circ/90^\circ$  base and in the  $-45^\circ/+45^\circ$  base. Additionally we did the measurements one time with using 4nm filters which preselect the entangled photon pairs (and which simplifies the adjustment of the source) and one time without the filters to get the maximal coincidence rate.

	Toptica DL 100 (original)	Violet-405 (new)
<b>Power</b>	10.2mW	11.7mW
<b>Coincidence rate with 4nm filter</b>	3000	2100
<b>Visibility <math>0^\circ/90^\circ</math> with 4nm filter</b>	99.1-99.2 %	97.4-99.3 %
<b>Visibility <math>-45^\circ/+45^\circ</math> with 4nm filter</b>	96.8-98.6 %	96.3-97.0 %
<b>Coincidence rate without 4nm filter</b>	11300	10950
<b>Visibility <math>0^\circ/90^\circ</math> without 4nm filter</b>	98.8-99.0 %	94.6-96.2 %
<b>Visibility <math>-45^\circ/+45^\circ</math> without 4nm filter</b>	98.0-99.2 %	86.8-87.4 %

**TABLE 3:** Comparison with the original laser system. Due to the bigger bandwidth we get a smaller coincidence rate and slightly worse visibilities.

### 3.2.6 Future development

- During adjustment it showed that beam quality is very sensitive to a relative rotation of the cylindrical lenses, so one could think about putting them into a goniometer mount for easier adjustment.
- One could think about adding further lenses in order to allow changing the beam waist without modifying its position. I think such a system would also be interesting for many other applications.

### 3.3 Beam Control Loop

As already mentioned we have to actively control our beam position in order to compensate thermal and other long-term drift effects. Within the lab these effects are fairly small, but even very simple tests (like opening the windows for some minutes) show that they have a strong influence on the long-term stability of the source. Figure (16) and (17) show the beam position drift depending on the room temperature. The beam position was measured by a long time measurement using the Spiricon CCD camera LBA-USB 620U. Additionally we measured the room temperature using a simple USB data logger.

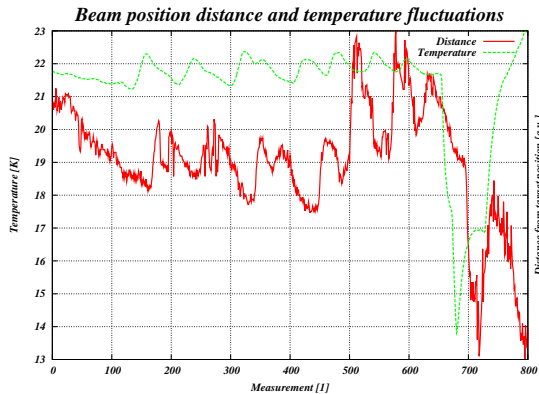


**FIGURE 16:** Measurement of the beam position drift with some external perturbations like a changing room temperature. In order to get a 2D plot we use the distance from the target position as well as the temperature.

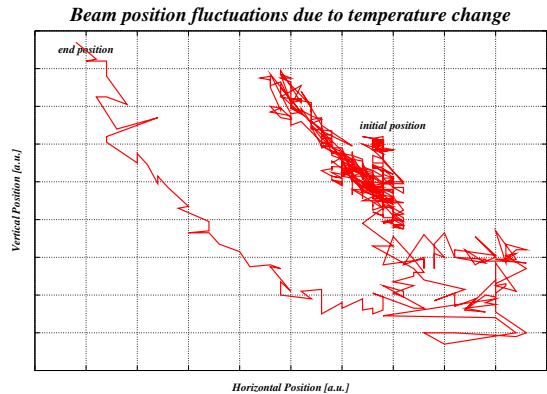


**FIGURE 17:** This graph shows the same measurement as on the one on the left, but this time we plot the horizontal and vertical position drift.

Due to our experience with other sources we hope that the biggest influence comes for the laser diode itself. This means that it should be enough to control the output beam direction directly after the laser diode. Other effects like thermal expansion of the nonlinear crystal, drifts of the mirror positions and so on should be negligible. If this assumption does not hold in the end one could put the whole source into a box and control temperature in order to reduce most of these other influences.

All the drift effects that we want to get rid of are rather slow. Thus it is sufficient to implement the control loop on default PC hardware using an external ADC in polling mode. This ADC reads the position of the laser beam from a position sensitive device (PSD), in our case a 4-quadrant-diode. Steering the beam is done via a special mirror mount equipped with two piezo-friction-motors that allow to tilt the mirror.

The next subsections will describe the used components in depth:

#### 3.3.1 The 4-quadrant-diode PDQ80A

The PDQ80A (see figure (18)) is a segmented quadrant position-sensing detector from Thorlabs. It works in a wavelength range from 400nm to 1050nm and includes a robust housing as well as a pre-amplifier and some other electronic circuits. A quadrant diode consists of 4 photodiodes that look like - as the name says - 4 quadrants of a circle. It is used to center the incoming beam to the center of the circle. The photocurrent of each diode is proportional to the overlap between diode area and laser beam. So in case of a centered beam the current of all 4 diodes should be the same.

In order to simplify use the included electronic circuit pre-amplifies the photocurrent and outputs the differences between right and left side or bottom and top respectively. An additional output give you the sum of all four currents. Using these output we only have to get the difference voltages to 0 in order to center the beam. Sign and amplitude of the voltages show us in which direction and how far we are away from the center.

A detailed description and specifications of the sensor can be found at the Thorlabs homepage

(<http://www.thorlabs.com/thorProduct.cfm?partNumber=PDQ80A>).

The photo-sensitivity of the sensor at  $400\text{nm}$  is about  $0.08\frac{\text{A}}{\text{W}}$ . With a maximal photocurrent of  $200\mu\text{A}$  this would lead to a maximal power of  $2.5\text{mW}$  and with a beam diameter of about  $1\text{mm}$  this would give a power density of  $320\frac{\text{mW}}{\text{cm}^2}$ . But on the other hand we have to consider the damage threshold of the sensor which is only  $100\frac{\text{mW}}{\text{cm}^2}$ . Thus we only can allow a power less than  $0.79\text{mW}$ . Choosing about  $0.5\text{mW}$  (which means that we have to attenuate our pump beam by a factor 200 by some ND-filters) we will expect a maximal signal voltage of about  $0.4\text{V}$  (the gain of the amplifier is  $10\frac{\text{kV}}{\text{A}}$ ).



**FIGURE 18:** *Thorlabs PDQ80A quadrant-photodiode*

### 3.3.2 The Labjack USB-ADC U3-HV

The Labjack U3 (see figure (19)) is a tiny and cheap USB measurement tool. It is very useful for some not very demanding control applications like our beam control loop. It can be easily plugged to every PC that is equipped with an USB port. Drivers are available for Linux and Windows and support polling as well as streaming mode of the device. It follows a list of features:

- 16 Flexible I/O (Digital Input, Digital Output, or Analog Input)
- Up to 2 Timers (Pulse Timing, PWM Output, Quadrature Input, ...)
- Up to 2 Counters (32-Bits Each)
- 4 Additional Digital I/O
- Up to 16 12-bit Analog Inputs (0-2.4 V or 0-3.6 V, SE or Diff.)
- 2 Analog Outputs (10-Bit, 0-5 volts)
- Supports Software or Hardware Timed Acquisition
- Maximum Input Stream Rate of 2.5-50 kHz (Depending on Resolution)
- Capable of Command/Response Times Less Than 1 Millisecond
- USB 2.0/1.1 Full Speed Interface
- Powered by USB Cable

Labjack also offers a HV version that supplies an input range of  $\pm 10\text{V}$  for the first 4 input channels.

Linux drivers and some easy examples are available (see [http://www.labjack.com/labjack\\_u3\\_downloads.php](http://www.labjack.com/labjack_u3_downloads.php) for a detailed list of available software and which features are supported). Unfortunately there is no COMEDI driver available, which would allow to stick to a standard interface.

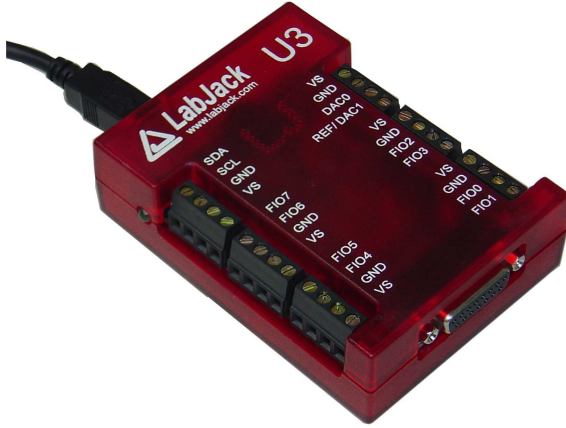


FIGURE 19: *Labjack U3-HV*



FIGURE 20: *Agilis-mirror-mounts*

### 3.3.3 The Agilis-mirror-mounts

We decided to use these piezo-motor driven mirror mounts (see figure (20)) because they are inexpensive and very compact. It is controlled by special driver that can be connected to the USB port of a standard PC. The driver applies special voltage signals to the piezo-crystal (in the simplest case a saw-tooth-signal) which lets the crystal expand and then contract again, but with a different speed. If you now put a plate next to the piezo it will go along with the expansion of the crystal, but when the piezo contracts very fast it will slip through due to its inertia. Doing more than one step allows to travel arbitrary length with a very high accuracy.

The big disadvantage of a piezo-motor is that friction is not the same every time and depends on many different influences (temperature, position on the crystal, speeds, direction, ...). Thus it is not possible to reproduce a former position with these mounts. But since we use it in a closed loop system we do not need this anyway.

Table (4) summarizes the most important features of the mirror mounts:

Features	AG-M050N	AG-M100N
Optic diameter	0.5"	1.0"
Angular Range	$\pm 2^\circ$	$\pm 2^\circ$
Adjustment Sensitivity	$2\mu\text{rad}$	$1\mu\text{rad}$
Maximum Speed	$1.5\frac{^\circ}{\text{s}}$	$0.75\frac{^\circ}{\text{s}}$

TABLE 4: *Specifications of Agilis-mirror-mounts*

### 3.3.4 The Agilis-controller UG-AC2 (UG-AC8)

The controller AG-UC2 (see figure (21)) allows to control the piezo-mirror-mounts manually or via a USB port. You can use an external power supply or directly power the controller via USB. If you use manual control there are three buttons for each axis and direction, which are related to different speeds of motion. If you hold down a button this will lead to 5/100/1700 steps per second respectively.

If you want to control motion from a PC there are some Windows drivers available. Since in our project we try to do everything with open-source software under Linux this option was not available for us. Thus we

implemented our own driver. Fortunately Agilis put an USB-to-serial converter chip directly behind the USB driver chip. Due to this there is already a generic Linux driver available that supports the converter chip. And the controller documentation gives detailed information about the command set that the controller supports. You can find a short howto in appendix [Setup HowTo for Agilis controller AG-UC2](#) that describes in detail how to setup the controller under Linux and also provides a simple `expect` script that sends commands and offers the possibility to check the reply for validity.



**FIGURE 21:** *Agilis piezo controller AG-UC2*



**FIGURE 22:** *Agilis piezo controller AG-UC8*

### 3.3.5 Sensitivity measurement

In order to implement a control algorithm we first have to do a measurement of the open-loop response. We also measured the number of coincidences during the scan, since this allows to get a feeling on how sensitive the whole system is to beam fluctuations. Therefore we use the ADC in polling mode and after 100 consecutive measurements we let the piezo motor do a single step. In order to center the coincidence peak we first search for the maximum and then do about 10 steps in any direction. If we then start our scan with a total number of 20 steps in the other direction the maximum will be approximately in the middle of our plot.

On the first scan without averaging (Fig. (23)) one could see that the resolution of the 12bit ADC is too low for clean beam control, because the signal fluctuations do not allow a clear assignment of the signal value to the corresponding step. This would lead to a restless system that moves a few steps forth and then back again only due to the measurement jitter. But fortunately our controlling task is not really time-critical and thus we can simply average over a certain amount of samples to improve our sensitivity. Figure (24) then shows the results that we got when averaging over 20 samples. The curve that we get is much smoother and one can see that the accuracy is now big enough to capture the individual steps of the piezo motor. This also means that the total accuracy of our controlling system is limited only by the actuator and not by the measuring device.

Additionally we can estimate the sensitivity of the source efficiency on the beam deflection. One can estimate that if we demand a maximal drop of 5% of the coincidence rate the beam must be only 5 steps away from the optimum. Therefore it is very important that the pump beam is controlled and also that we use single steps for this task in order to reach a high stable efficiency of the source.

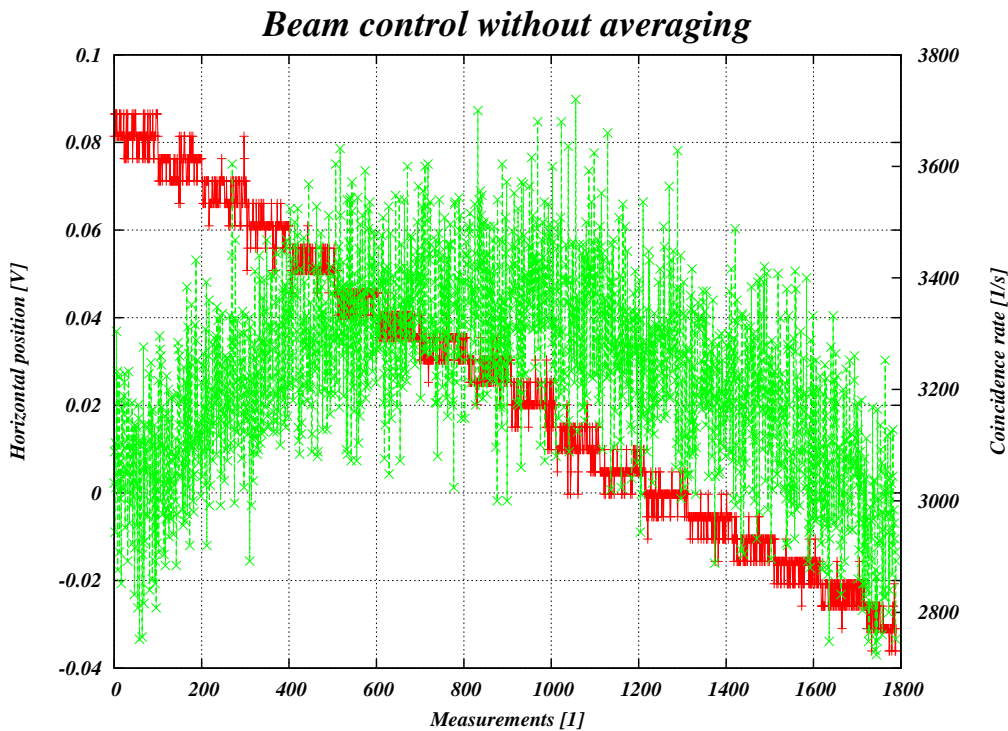


**FIGURE 23:** *Laser control without averaging: every data point is plotted with leads to a very noisy graph.*

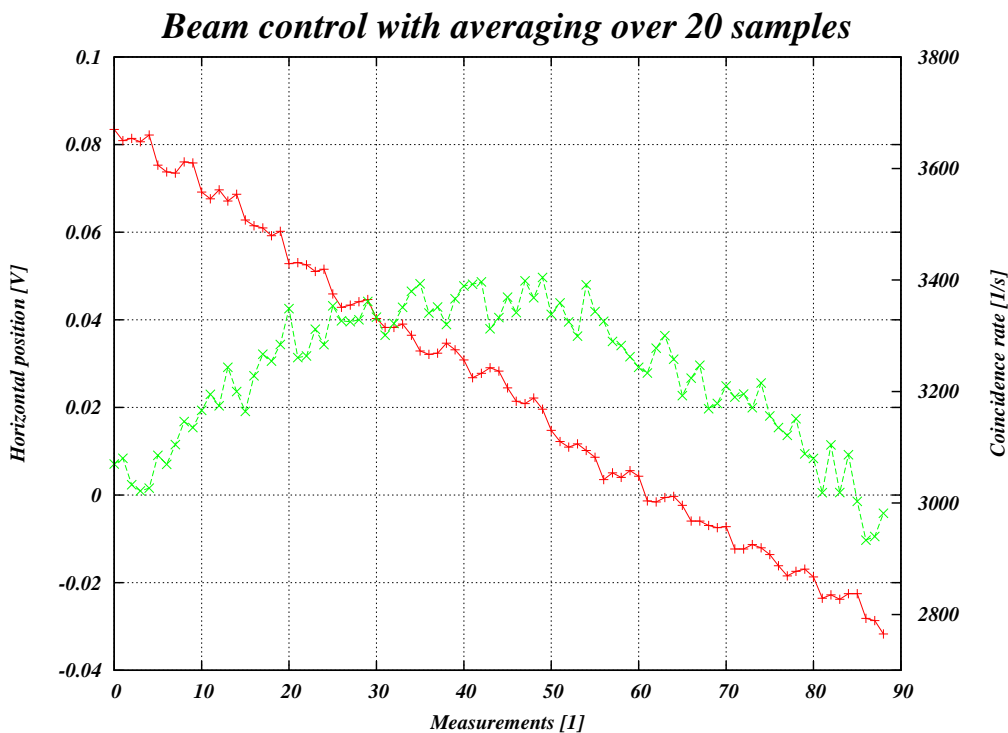


**FIGURE 24:** *Laser control with averaging over 20 samples flattens the curve and allows to use the calculated mean values directly for the control algorithm.*

Note that these scans were done during testing of the control-loop. At this time the controller mirror was located after the focusing lens system, which allowed to stir the beam without reducing its quality. In the final setup the beam will be once adjusted and then the control loop will be activated to keep it in position.



### 3.3.6 The control algorithm

Currently we only use the Labjack's first 3 analog input ports as well as the internal temperature sensor in polling mode. With a sampling time of approximately 1ms for each channel this gives a scan frequency of about 250Hz. Timing could be improved using streaming mode of the device but this would result in a more complex code and is not necessary for our current task.

Since we only use an 12-bit ADC a single measurement is not very accurate. Thus we average over 20 measurements to reduce noise and get reliable position values. Subsequently we divide the position signal by an average step-size (which is different for X and Z axis) and get the number of steps that are in theory needed to get to the origin. Using this simple algorithm works very well except for frequent single steps that occur due to fluctuations about the target position. Thus we only make steps if we are more than 2 steps away from 0.

Long time measurements of the beam position show that under laboratory conditions the control-loop is almost not required, but as soon as some unexpected external influences like temperature differences, shocks and so on occur, it will be essential for the performance of the source. The action of the control algorithm is visualized in figure (25), which shows the temperature as well as the number of steps necessary to hold the initial position. If you compare these steps with figure (24) you see that this would lead to almost zero efficiency without the controller.

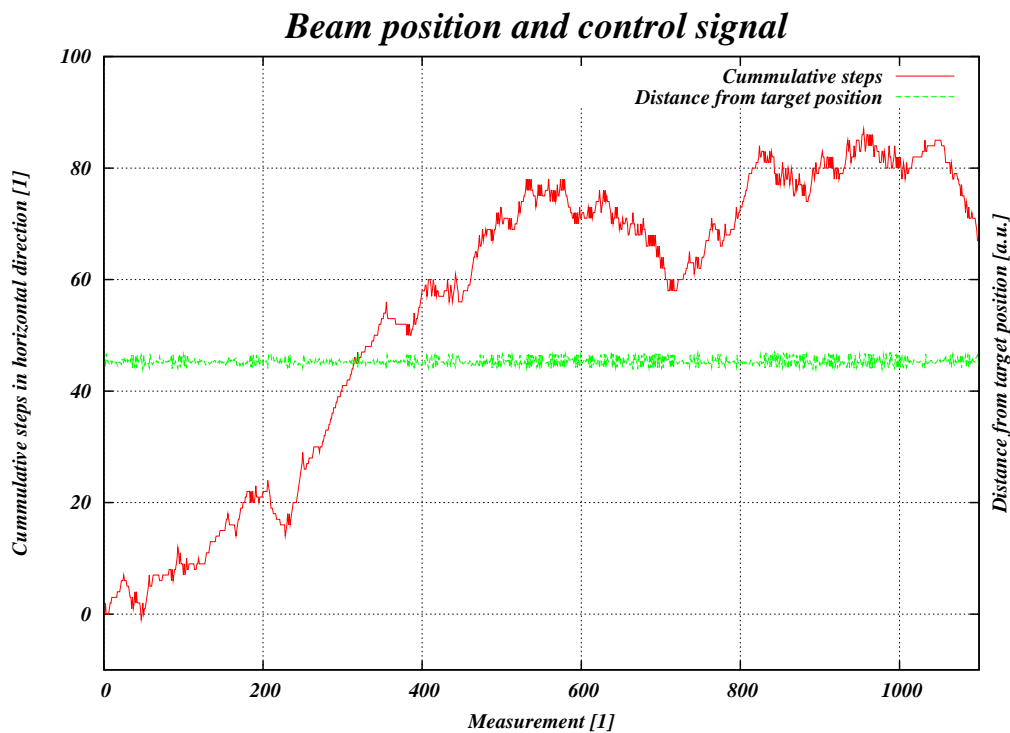


**FIGURE 25:** Pump beam control during temperature change. You can see that the beam remains at its target position as well as the number of steps done by the controller.

### 3.3.7 Future development

- A very simple improvement would be to switch to a 14bit ADC in order to improve sensitivity and to allow control without averaging over many samples. Additionally one could use a voltage range of  $\pm 2.5V$  which would better match to the signal created by our 4-quadrant-diode. This way the accuracy of the measurement system could be further improved.
- Another degree of freedom that is still available is the beam size which is related to the distance of the PSD from the BBO. A larger distance would firstly lead to a bigger lever and therefore result in a better accuracy of the measured beam deflection angle. Additional to this geometrical effect the measurement accuracy would also be influenced by the fact that a bigger beam size would allow to use more intensity and thus create a bigger output signal.
- Switching to a different ADC would also allow to select a device that is supported by the COMEDI project. This would allow to write a more general driver that will be easier to maintain in the long run.
- In the final setup the control algorithm should be implemented on an embedded board (FPGA board) instead of a standard PC, but this should not be a problem at all.
- The control algorithm itself could be optimized. For example a self calibration would be reasonable. This algorithm would automate the sensitivity measurement if its preset values lead to bad behaviour. This would simplify making changes to the setup where the distance between controlled mirror and PSD has to be changed. One problem would be that the recalibration would be done at random times and thus could interrupt some running measurements.

## 3.4 Pair creation and walkoff compensation

### 3.4.1 Theoretical considerations

As already described in section [Walkoff Compensation](#) the walkoff compensation consists of a half waveplate and a second BBO of half length after the first BBO. This system corrects the longitudinal walkoff completely as well as the transversal walkoff by part. The typical setup used two separate BBOs for each path (Alice, Bob) after the pump beam was blocked. In our setup we tried another version. We put the waveplate and one second BBO directly after the first BBO. This has the following consequences:

- We need only one compensation crystal. This makes the source less expensive because the BBO crystals are some of the biggest matters of expense. Additionally we can make sure that small difference of the crystals (a slightly different cut-angle, ...) do not occur.
- We make sure the beam passes the compensation crystal at the same angle as the original crystal. Since the angle is only about 3 this influence will not be too big but should also be mentioned.
- Of course everything you do has also some drawbacks. In this case it is the problem that the pump beam also passes the second BBO and creates photon pairs. The beam cannot be blocked since we need it for the beam control loop. First tests swapping the BBO setup in the running system showed nearly no influence on the detected photon pairs, but it cannot be denied that it could complicate the initial adjustment of the system. But since the pump beam is focused on the first BBO the pair creation in the second one would be less probable. Additionally we can simply block the pump beam after the first BBO during initial adjustment and only remove the beam block for continuous operation.

### 3.4.2 Practical considerations

As with the focusing system we try to put all components in a cage system to make the system stable and compact. The rotation and tilt angle of the first BBO are not crucial for the initial adjustment. Thus we can place it in a simple cage rotation mount. For a later fine-tuning of the source the angle if the pump beam can still be adjusted. The same is true for the half-waveplate. The second BBO is a bit more complicated. The created two-photon-state looks like  $|\psi\rangle = |HV\rangle + e^{i\phi}|VH\rangle$ , and the phase between the two terms can be adjusted by the relative tilt angle between the two BBOs.

### 3.4.3 Measurement of the ring system

In order to receive an impression how the pair creation looks like with our broadband laser we decided to take a picture of the ring system (Fig. (26)). Therefor we created a simple lens system that maps the ring system onto the CCD chip of our camera in its actual scale. As you can see from the lens equation  $\frac{1}{f} = \frac{1}{b} + \frac{1}{g}$  this can be achieved by locating CCD chip  $b$  as well as the imaging plate  $g$  at a distance to the lens of  $2f$ .

In our case we used a 40mm lens and mounted it in a lens-tube approximately 80mm away from the chip. We also put some long-wave pass filters into the tube in order to filter the ambient light and increasing the signal-to-noise ratio that way. A 6nm bandpass filter is used to select the rings with the correct wavelength. By adjusting the distance of CCD camera and the lens tube we can choose our imaging-plane and thereby how large our ring system will be in the picture.

As already mentioned before we also get a another ring system from the second BBO(Fig. (27)). So in a first run we block the pump beam in front of the second BBO in order to prevent this and to get one pure ring system:

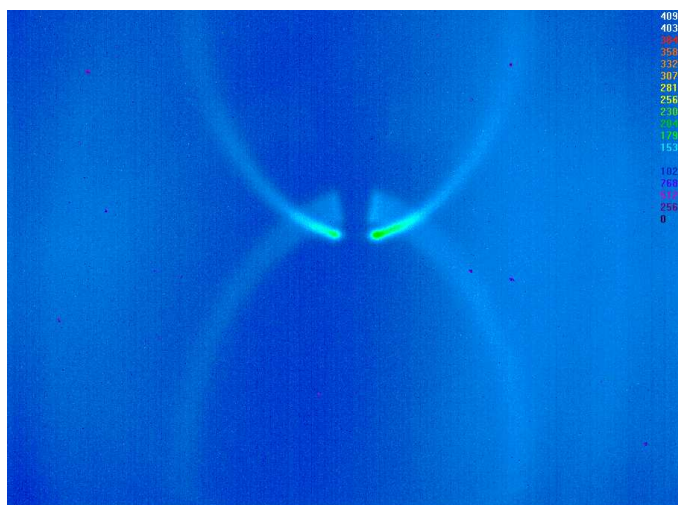


**FIGURE 26:** *Picture of ring system from a single BBO. The pump beam was blocked in front of the second BBO. A 6nm bandpass filter was used to select the rings with correct wavelength.*

Finally we also took a picture of the full ring system.



**FIGURE 27:** *Picture of ring system of the full setup. A 6nm bandpass filter was used to select the rings with correct wavelength.*

#### 3.4.4 BBO characteristics

In our setup we use a 5x5x4mm BBO for pair-creation and a 5x10x2mm BBO for walkoff correction. Beta-barium borate ( $\beta - BaB_2O_4$ ) has the following important properties:

- Broad phasematching range ( $\approx 400 - 2000nm$ )
- Useful optical transmission ( $\approx 200 - 2000nm$ )
- Large effective nonlinear coefficients
- High laser damage threshold
- Low thermo-optic coefficient

### 3.5 Coupling Optics

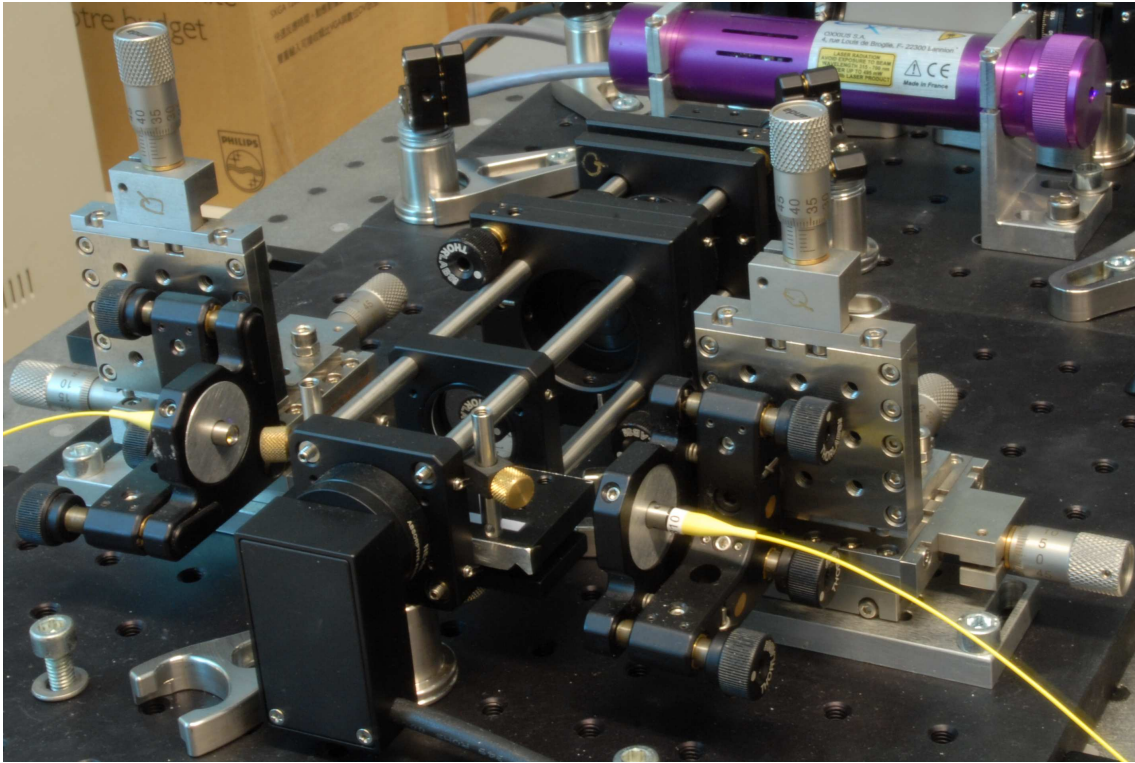


**FIGURE 28:** *Picture of the coupling system. The manual translation and tilt stages can be replaced by motorized versions for automated coupling.*

#### 3.5.1 Theoretical considerations

In order to select the correct photons we use a single mode fiber and a focusing optics. If you light back through the fiber the beam that the focusing optics creates matches the mode that will be accepted by the single-mode fiber during operation. The needed beam parameters can either be calculated theoretically or measured it by optimizing the source efficiency.

We did this measurement using an older version of our EPR source. The focusing optics consisted of a single lens. The degrees of freedom that we have are the angle and position of the fiber as well as the distance of the lens from the fiber. The optimization can be done by choosing a different distance from the BBO to the coupling optics. Then readjust the lens position and angle. This is very time consuming and a not really reproducible task. The problem is that you cannot be sure that you are in a global maximum and that you have many coupled degrees of freedom. Thus we only checked a very small region around the empirical values known from the old version of the source in the first run.

But we also have an idea how to improve this problem: By using a slightly more complicated version of the coupling optic one could simplify or even automate parts of this optimization. This works in the following way: We place an additional lens after the BBO, where the distance to the BBO is equal to the focus length of the lens and the axis of the lens matches the pump beam. This setup has two effects:

- The photon beams get **recollimated**, which allows to couple them into the single mode fibers using default fiber collimators. Beam characteristics can be selected by simply changing the used collimators. But of course there is also a drawback: You cannot change the beam continuously, but only in steps corresponding to the available collimators.

Another problem could be that the beam quality decreases because the beam does not got through the lens' axis. But the actual quality can simply be measured by lighting back through the lens system and using the CCD camera.

- The photon beams are deflected so that they are **parallel to the pump beam**. This can be seen using simple geometrical optics. Beams with origin in the focus of the lens will be mapped into parallel beams. Due to lens errors and Gaussian beams this will not be exactly true but it will be a good approximation.

The big advantage that we now have is that the optimal angle of the fiber does no longer depend on its current position. In theory there should be one optimal angle (when the collimator axis is parallel to the pump beam). And the remaining optimization of the lens position is completely independent of its angle. In this way we achieved to decouple some of the degrees of freedom of the system (see figure (29)).

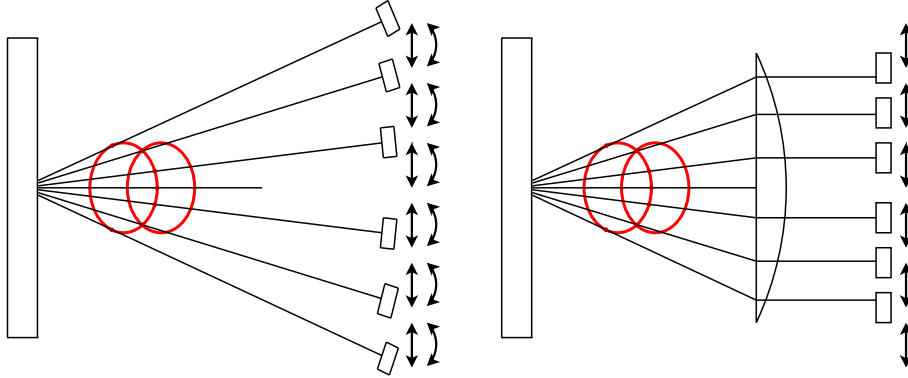


**FIGURE 29:** *Design of the coupling system using 2 lenses. You can see that using 2 lenses leads to a decoupling of the translational and tilt degrees of freedom. Additionally standard fiber collimators can be used as second lenses which further simplifies the adjustment.*

Testing this system in practice showed that it simplifies adjustment and that it should be easy to automate the whole coupling system.

### 3.5.2 Practical considerations

Due to our requirements aiming for a small setup we use a 100mm plano-convex lens, which is placed within the cage system of the BBO. This makes sure that the optical axis of the lens matches the pump beam. Some tests show that the exact distance from the BBO only has a minor influence on the performance of the coupling system. The whole cage system is very stable and simple to adjust. We also added some slots for filters or apertures that can be inserted into the cage system during operation.

**Apertures** can be used to do a **coarse pre-selection** of the entangled photon-pairs as well as to **block scattered light** from getting into the single-mode fiber.

Different filters can be used for some tests during operation (for example to check whether the photons have the correct wavelength). Additionally we have to use bandpass filters during adjustment of the source to couple in only the entangled photon pairs. In the old source these filters were located directly in front of the single-mode fiber. Now we have the possibility to put only one filter directly after the BBO with the following results:

- Using only one filter prevents errors from slightly different filter characteristics in both paths.
- Filters are very easy to plug-in and out during operation.
- Filters could conceptually belong to the source and not to the measurement system.

The last part of the coupling systems are default fiber collimators which are mounted in a mirror holder on two translation tables. For our tests we use manual versions but in the final version of the source we will use stepper-motor controlled translation stages as well as a piezomotor driven mirror mount in order to automate adjustment as well as to compensate small drifts.

Another minor change that we did was to place the colored glass filters that reduce the influence of the ambient light after the single-mode fiber within the measurement system and not in front of it. The reason why we did this is because the glass filter creates a small beam offset and a single mode fiber is much more sensitive to such offsets than a multi-mode fiber. So if you locate your filter in front of the single-mode fiber you cannot simply remove it during operation without readjustment of the coupling system.

### 3.5.3 Automated coupling

We decided to use steppermotor controlled stages for the translation because they are easy to control and very cost effective. The bigger size compared to piezo versions is no problem for us and therefore we have the additional advantage that these stages offer very good reproducibility as well as nearly no hysteresis.

We decided to use the following stages from Standa, which we control over a simple serial port protocol from our lab PC (see figures (30) and (31)):

Model	8MT184-13
Travel range	13mm
Resolution	1.25 $\mu$ m
Lead screw pitch	0.25mm
Weight	0.25kg



**FIGURE 30:** *X-Translation-Stage 8MT184-13 from Standa*

**TABLE 5:** *X-Translation-Stage*

Model	8MVT40-13
Travel range	13mm
Resolution	0.021 $\mu$ m
Lead screw pitch	0.25mm
Worm-gear ratio	60 : 1
Weight	0.45kg



**FIGURE 31:** *Z-Translation-Stage 8MVT40-13 from Standa*

Unfortunately due to some technical problems physical implementation of the control loop was delayed, but we did some theoretical considerations about the automation. First of all if the source is already adjusted we have the advantage of our system that all degrees of freedom on one side of the source are decoupled. So one could use a simple hill climbing algorithm and optimize for the single rate. Adjusting this optimum on both sides should automatically give a global optimum for the coincidence rate.

In practice one could perhaps get better results if one uses a global hill-climbing algorithm that optimized

directly for the coincidence rate. The only problem is that you already have to be near the optimum in order to see any coincidences. The solution could be to define a heuristic cost function that contains single as well as coincidence rates and optimize for this cost function.

One problem with such a system is that you could only find local maxima and that you have to be near to the maximum for the algorithm to work. Since we theoretically have only one maximum the first point does not matter for us, but the second point is very important. It will not be possible to automate the complete adjustment process, but only the fine-adjustment and stabilization of the coupling system over time.

For the final operation of the source this is not a very big drawback, but for the development and testing of the source this would be an important feature, because it would make all measurements reproducible. It could be that the algorithm or the controlling elements are not suited to find the real maximum or even worse that it finds different maxima starting from equal initial conditions. But all these effects should be perfectly reproducible by doing a statistical evaluation. The average coincidence rate that you get will not be the absolute maximum rate that is possible but it will be the rate that is important for the practical use of the source. It will tell you the average rate that you can expect from a fully automated source as well as the standard deviation from this average.

The design of our coupling system will also help us implementing the coarse adjustment of the source. Since all degrees of freedom are decoupled one could randomly search for a significant single rate around the initial position. The search radius can be expanded until something is found. To find the approximate initial position by hand we can add some apertures to the BBO cage system that preselect the entangled photons. One can then do the initial manual adjustment by lighting back through the single-mode fiber and align them to these apertures. One problem that we will have is that the motion of the piezo driven mirror mount is not reproducible and thus it will not be possible to return to the initial setting. Therefore we will have an incremental error that will offset the center of our random search. We hope that our algorithm will reach the catchment area before the incremental error gets too big, but this can only be shown in the experiment.

### 3.5.4 Measurement of the coupled beam profile

In order to compare the old and the new coupling system as well as to select a proper fiber collimator for the new system we measured the beam profile that we get if we light back through the single-mode fiber. As already mentioned we use the values that we got from the old coupling system as a reference.

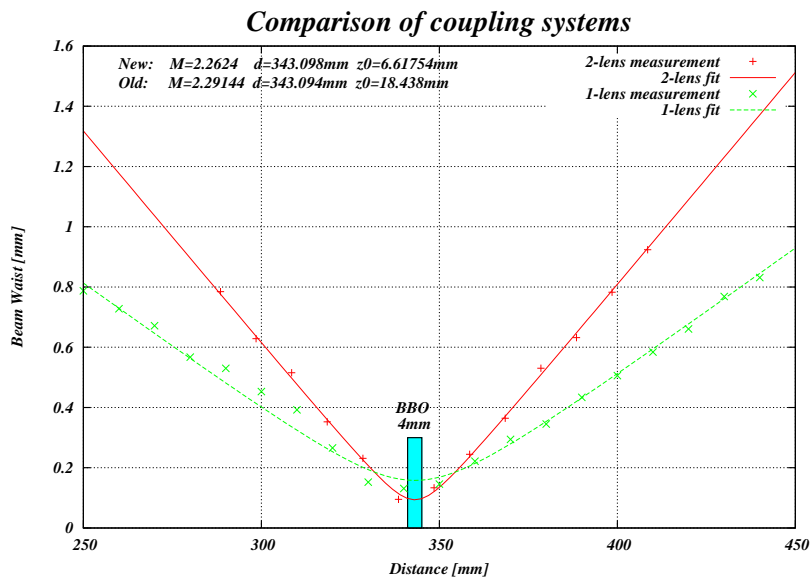


**FIGURE 32:** Comparison of the old and new coupling systems. The new system has a smaller beam-waist which means that we will have a lower coincidence rate but a better visibility. The focus position  $d$  is almost the same in both systems.



This measurement (Fig. (32)) showed that the used collimator leads to a smaller beam waist than the reference coupling system. This could be changed by ordering different collimators, but since it is always a trade-off between count rate and visibility we decided to stick with this collimators and have in mind that our count rate will change slightly.

### 3.5.5 Comparison with the original coupling system

In order to compare only the coupling systems we optimized the original source first and then only replaced the coupling system. After some optimization we got the results shown in table (7):

	Original	New
<b>Single Rates A/B</b>	33000/31000	35600/32500
<b>Coincidence Rate</b>	3300	2400
<b>Visibility 0°/90° with 4nm filter</b>	99.2-99.8 %	99.3-99.8 %
<b>Visibility -45°/+45° with 4nm filter</b>	95.9-97.6 %	97.9-99.0 %

**TABLE 7:** *Comparison with the original coupling system*

You can see that the coincidence rate of the new system is worse whereas the visibility is better. As already mentioned it will always be a trade-off between these two values and only the user can say what he prefers.

### 3.5.6 Future development

- **Automated coupling:** This would simplify the source development a lot and would also allow to do reproducible and reliable measurements.
- **Different collimators:** With the automated coupling it would also be easy to do a series of measurements using different collimators.
- **Single photon spectrometer:** Measurement of the single photon bandwidth should show the dependence on the used beam waist as predicted by equation (32).



## 4 Measurement system

This section contains the second part of our setup - the measurement system. This measurement system basically consists of single photon detectors as well as a coincidence logic that allows to detect coincident events. In order to determine the quantum-state of the created photon pairs we additionally need some polarizing elements that allow us to measure the projection of the system state onto some arbitrary bases. We can then reconstruct the quantum state from a series of measurements, whereas it is not possible to directly measure the state.

In the following subsection I will describe all components that we need for an automated quantum-state-tomography. I will put emphasis on the parts that were implemented during this diploma thesis.

### 4.1 Single photon detectors

One of the most essential parts of our measurement system are the single photon detectors. We have to work with single photons because only then we see quantum effects. If we would average over a number of photons we would only get classical behaviour of the system. This single photon detection can be achieved by an avalanche photo-diode (APD). This is a semiconductor diode that is applied with a high reverse bias voltage of up to 50 volts. This means that if any free charges are created within the junction an avalanche will be triggered and an internal current gain effect takes place.

Now one uses the photo-electrical effect to create an initial charge and it will be possible to measure single photons. Of course it is also possible that some free charges are thermally-induced which leads to a certain dark-count rate that is also present if there is no incident light.

For our setup we use the 4 port single photon counting module array SPCM-AQ4C from PerkinElmer (Fig. (33)).



**FIGURE 33:** *PerkinElmer SPCM-AQ4C 4 port single photon counting module array*

Photon detection efficiency at 830nm	35-45 %
Operating temperature	5-40 °C
Maximum dark counts / sec. (per channel)	500
Typical dead time	50ns
Maximum continuous count rate (per channel)	1.5 Mc/s
After-pulsing probability	0.3-0.5 %
Timing jitter (according to [20])	640ps

**TABLE 8:** *Specifications of PerkinElmer SPCM-AQ4C 4 port single photon counting module array*

The next important diagram shows the spectral efficiency of the detector module. As you can see there is an of a few percent in the range around our pump beam wavelength which means that we have avoid that even small fractions of the pump light reach the detector module. Our photon pairs with 810nm wavelength are not directly at the maximal efficiency of the detector but still near enough to get a sufficient performance. Due to the fact that the efficiency further decreases with higher wavelengths we can use simple long-wave-pass filter to cope with the ambient light.

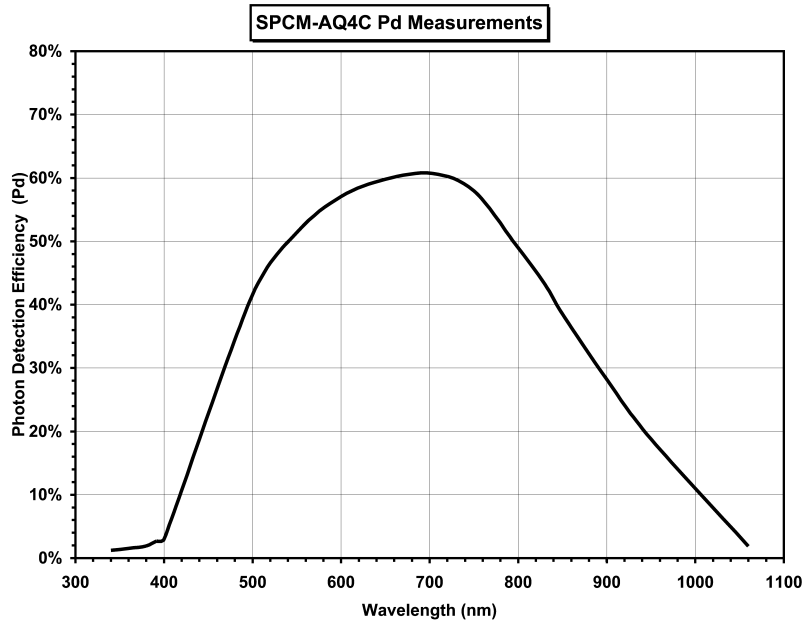


**FIGURE 34:** *Spectral efficiency of the PerkinElmer single photon counting module*

### 4.1.1 Measurement of the detector offsets

During the first measurements with the new detector module we found out that there is an offset between the different channels. Fortunately we can measure this offset by using our timetagging module (see in the next section) and do a coincidence measurement of the photon pairs. Plotting the arrival time differences in a histogram then shows a peak at the offset of the two involved channels. Using different pairs of channels allows to determine the offsets of all channels compared to the first one.

The measured offsets of our specific detector module can be found in table (9):

Channels	Offset [ns]
0 → 1	5.9
0 → 2	0.6
0 → 3	4.7

**TABLE 9:** *Channel offsets of PerkinElmer SPCM-AQ4C 4 port single photon counting module array*

The offsets seem to be constant over time and other environmental influences (at least over a period of a few months within our laboratory) so it is very easy to compensate them. One could simply add some pieces of wire with the correct length to the setup or if using a timetagging system this could also be done in software.

## 4.2 The timetagging module TTM8

For most applications of entangled photons it is essential to detect coincidences. Because you always have unwanted single photons detected where the second photon is missing and only looking for coincidences is a very efficient way to get rid of them. At the beginning of this project we used a simple AND logic with a hardcoded timing behaviour. This logic counts a coincidence if within a certain time interval (in our case 4ns) there are signals on two channels. Such a logic is very easy to build and also very fast.

During the project we replaced this logic by a timetagging system. This means that we have a timetagging module with a precise internal clock and each detection event is tagged with the time of its arrival. All events are then sent via a network connection to our lab PC where they are analyzed and the number of coincidences is calculated. There are the following reasons why we prefer this more complex system:

- We have the freedom to choose our time window as we like. The size of the coincidence window will determine the number of accidental coincidences that we measure. These are created by single events on both sides that happen at the same time by accident. The rate of such accidental coincidences can be calculated by the following equation:

$$C_{acc} = S_A \cdot S_B \cdot t_c \tag{45}$$

where  $S_A$  and  $S_B$  are the single rates of both channels and  $t_c$  is the coincidence window. One can understand this expression the following way: The first event determines the position of the timeslice. The possibility that an event on the other channel is detected within this timeslice is only depending on the average time between two events  $S_B^{-1}$  as well as the size of the timeslice  $t_c$  and is given by  $S_B \cdot t_c$ . Multiplying this probability with the number of events on the first channel finally gives the estimated number of accidental coincidences.

We can conclude from this equation that for higher single rates these accidental coincidences will become a problem.

- We can now measure the offset between two channels and also correct it by software. Such an offset can be created by different path length or as we already mentioned in section [Measurement of the detector offsets](#) by the detector itself. It also allows a fast check whether all coincidences are measured, whereas in the old system you could only try other offsets and look if the results get better or worse. So in fact it is a big simplification for the practical work with the entangled photon source.
- Software development is easier because data analysis is done in a high level script and not in hardware. For example all the tools that I implemented to calculate the coincidence rate as well as to measure the channel offset are simple Linux bash scripts. It would also be easy to implement new checks for example for double pairs or after pulses which could lead to bad results if not compensated.
- For the application in a QKD setup it is important to mention that using the timetagging module would allow to detect a time-shift attack as described in [21], which would otherwise be a serious security risk.

#### 4.2.1 Hardware



FIGURE 35: *Timetagging module TTM8*

The timetagging module mainly consist of a **precision clock** with a resolution of 82.3ps, which is much lower as the timing jitter of the detector module and thus does not restrict the total accuracy of the measurement. It offers **8 input channels** with a supported total rate of up to 30 Mcounts. The captured timetags are then sent to the lab PC via a gigabit ethernet connection. Therefor a UDP packet is sent whenever an ethernet jumbo frame (up to 9000 bytes) is filled. Additionally there is a hardware timer that allows to specify a timeout for the packet transmission. This is needed during source adjustment when you have very low count rates. Otherwise it would not be possible to get an online display of the current count rates.

#### 4.2.2 Software

First of all I will describe the state from which we started when the project began. There were already some software components available that should be reused if possible. Unfortunately this was not possible without some modifications:

- `coincgw`: This is the first part of the user interface of the coincidence logic that already worked with the old version of the coincidence logic. It directly reads from the serial port where the coincidence board is connected and provides the data via two UDP ports (one in ASCII format and one in binary). It allows several consumers to read the data simultaneously.
- `coincdisp`: This is the second part of the user interface. It provides the graphical window and displays the measured rates in realtime. Additionally some easy calculations are done like averaging over some samples, visibility in different bases, summation over all channels. See figure (36).

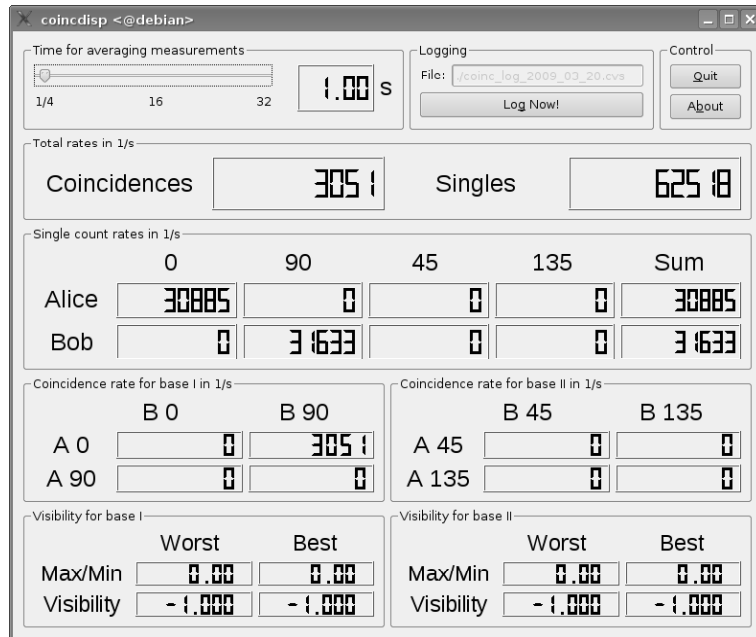


**FIGURE 36:** Screenshot of the graphical user interface `coincdisp`. In this picture only the Alice  $0^\circ$  and the Bob  $90^\circ$  detectors are used, which is enough for source adjustment. But the same tools can be for a full QKD systems with 4 detectors per side.

- `qeval`: This is a low level data analysis tool written by Bernhard Ömer during a long range entanglement experiment [22] that was originally used for the free space distribution of entangled photons. It automatically corrects detector offsets and works together with a QKD stack. Since it reads input data from two separated data files it also allows to use the separate timetagging modules for data acquisition which is very important for practical systems. But for our current task we only need a small part of the features that it supports. And we also had to add some small changes in order to get all the data that we needed out of the program. For future development it would be very interesting to rewrite this tool in a way that it fits to the current needs.

These are the foundations around which we will build our toolchain. The development version of all tools will be implemented as small Linux filter application that use standard input and output if possible. This allows to use default Linux tools between the tools in order to add some data modifications or the like. For example it would be possible to log the data stream to a file after each stage of the filter queue. This is very helpful for debugging and testing new software components without the need for new measurements. Additionally we use a few shell scripts that allow to start the measurement system with a single command without many options. The following list shows all the tools that I implemented:

- `ttdump`: This is the first stage in the filter queue. UDP datagrams are read from a socket. The header is interpreted which allows to detect missing packets as well as the firmware version of the timetagging module. The rest of the packet data, namely the timetags, are passed on to the standard output.

Since this task is very simple and general we first tried to handle it by using the Linux tool `nc` but we had some troubles with the alignment of the data. Using a selfmade tool also has the advantage that error detection is much easier.

Dumping the created output stream into a file allows to store the full history of the detected photons. You can then use a stored datafile to develop some high level algorithms like QKD stack or the like and finally directly pipe the acquired data into this application to get a running system.

- `tt_coincgw`: The simplest task that can be done with the timetagging module is calculating single as well as coincidence count rates and display them. This is especially needed during source adjustment. As already mentioned we want to reuse the `coincdisp` user interface for this task.

Therefore the tool first reads the timetags from standard input and counts the single rate for each channel. Since the timetags are almost ordered we can simply check whether the difference between two consecutive timetags is smaller than the coincidence window in order to detect coincident events. Due to the fact that the channels are not read at equal times but sequentially sometimes it can occur that two timetags are swapped. This problem is cached by simply taking the absolute value of the difference.

Finally the measured count rates are printed to standard output in ASCII format or in binary, depending on some parameters. As you can see this tool does not use an internal timing which is very important for reproducibility. The same input data always gives the same output independent of the speed of the PC or the small fluctuations of the runtime of different instances.

Since the binary format does not match the original format of the coincidence logic we had to add this `raw` format as an option to the `coincgw` application. This application can now directly read from standard input and provide the count rates. One problem that we have is that we now need an additional timer that allows to update the display if no event occurs at all. This leads to the problem that both clocks (the PC clock and the clock of the timetagging module) drift apart and there is a certain probability that for a short time the display shows wrong values. Choosing a high update rate mitigates this problem in practice.

Logging data in this stage has the advantage that you need considerable less memory and you can use a human readable format. Of course you lose the full history and only store mean values which prevents the data from being used for any further event-based calculation.

- `tt_to_qlval`: As already mentioned `qlval` is a very powerful tool that works together with a QKD stack and also does a lot of statistical checks on the data. Since it was developed for transmission of photons over wide ranges where you have very small count rates it is based on input files instead of streams. This offers the possibility to reuse data and use it for different calculations. Since we have very high count rates in our current experiment this design is not well suited for our task, but even so we want to add the long list of features that `qlval` provides to our toolchain.

For future systems it would be very useful to redesign the toolchain so that it offers automated offset detection as well as a distributed data acquisition but is more suited for current systems.

- `tt_analyser`: This was a first example to implement an automated offset detection before I heard about `qlval`. It simply calculated the difference between two consecutive timetags and prints it to standard output in an ASCII format. Together with some default math tools (in our case `R`) it allows to plot a histogram of the arrival time differences. This is exactly what you need in order to determine the offset between two detectors. Although you could also use `qlval` to do this task automatically it is sometimes very useful to look at the histogram yourself. Currently this is only a small helper application, but as already mentioned this should be changed in the future.



### 4.3 The quantum state tomography stage

In order to characterize our entangled photon source we want to determine the full density matrix of the system. Of course this is an abstraction of the real system but quantum algorithms only consider the density matrix and thus it is very important for us to measure it in an efficient way.

The theory of how to reconstruct the full quantum state from individual projective measurements has already been discussed in [Quantum state tomography](#). In this section we will focus on the physical implementation of the measurements as well as on the software components that do the actual reconstruction.

#### 4.3.1 Design

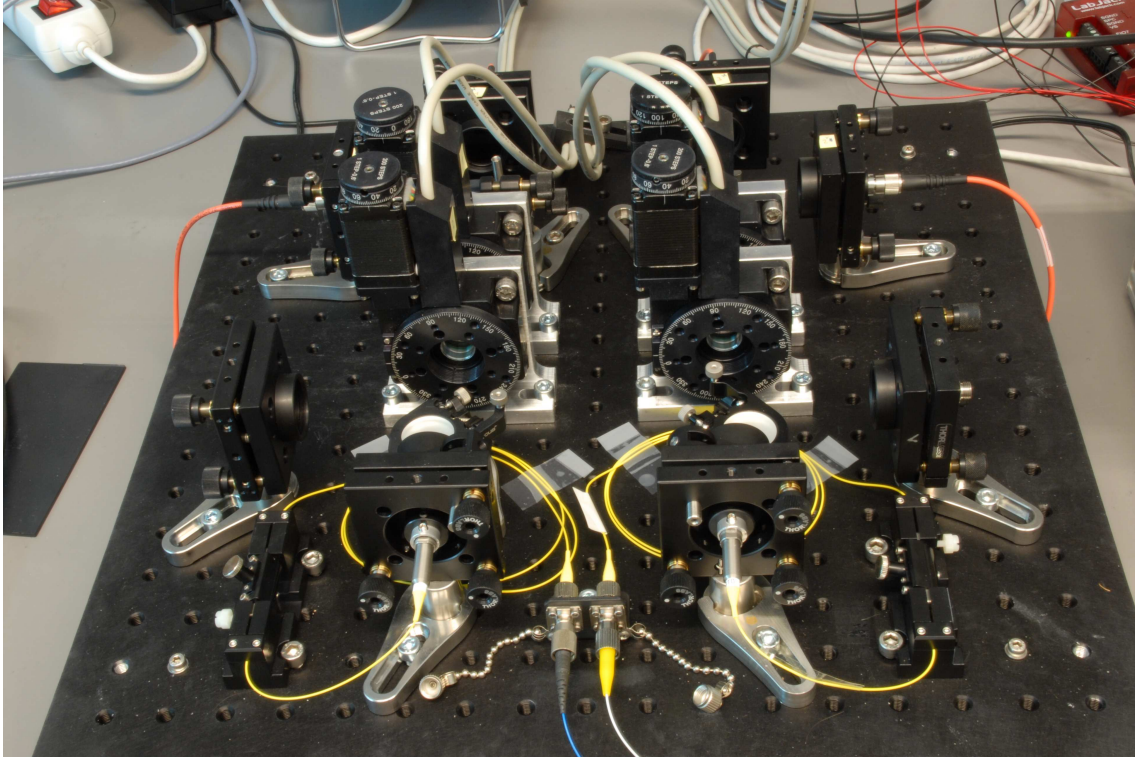


**FIGURE 37:** *Quantum state tomography stage*

The design of the tomography stage (see Fig. (37)) was based on the idea that we want to have as much freedom in measurement as possible. This results in a bit more complexity as it would be needed for a final product, but it also allows to get a feeling for the state tomography and test a lot of different measurement scenarios. I will now list a number of features that we wanted to implement:

- **Long-wave pass filters:** In order to filter as much of the ambient light as possible the filters are mounted **directly in front of the multi-mode fiber** that leads to the single photon detector. We use FGL665 colored glass longpass filters from Thorlabs that block light with a wavelength lower than 665nm as you can see in figure (38):

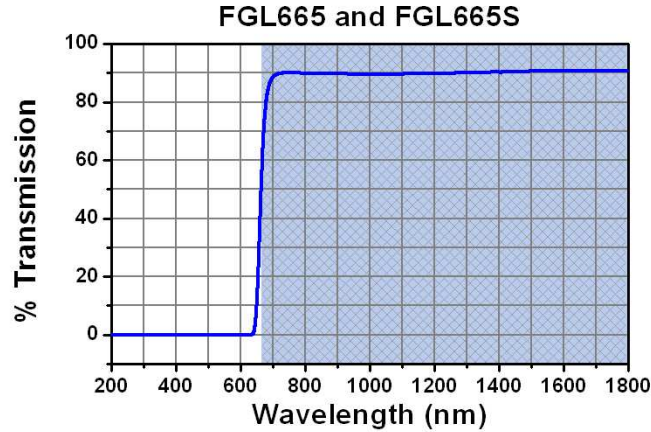


**FIGURE 38:** *Transmission curve of the ambient light filters*

The ambient light with longer wavelengths does not have much influence on the countrate because the single photon detectors have a much lower efficiency in that region (see Fig. (34)). The advantage of these long-wave pass filters compared to some bandpass filters is that they have a very regular pass band. The remaining losses of about 10% could be avoided if using a coating for the specific wavelength that we have.

- **Direct path:** In order to measure the incoming photons directly without any projection we added an additional path which can be selected by a flipping mirror. For the final setup this path can be replaced again but during adjustment it allows to check the relative efficiency of the projecting paths. Additionally it is needed to adjust the source if you only have two single photon detectors. Because in this case you need to optimize the total single and coincidence rate.
- **1 or 2 detectors per side:** Using a polarizing beamsplitter(PBS) as our polarizing element allows to use either one detector per side or two. But therefore we have to cope with crosstalk (photons are passed on to the wrong path) as well as a worse extinction ration (about 1:1000).
- **Selectable bandpass filters:** We place our 4nm filters directly after the single mode fiber. In that way we only need one pair of filters for all paths that we have. Additionally we mount the filters in a flipping mount that allows to simply remove the filters during operation.
- **Freely selectable measurement basis:** In order to achieve this we mount waveplates in motorized rotation stages. Using one quarter waveplate and one half waveplate on each side allows us to choose any desired measurement basis. Theoretically we only need a few bases for the quantum state tomography but with this system we have the opportunity to do a lot of additional tests that would not be possible with a fixed set of bases.

In order to fulfill all these requirements our measurement system has to be more complex than it must be in the final setup. Thus there are still a lot of optimization capabilities for future development. Currently the setup is designed to offer a broad spectrum of possibilities and not to do one specific measurement in the most efficient way. Figure (37) shows the physical implementation of the tomography stage whereas the design is shown in figure (39).

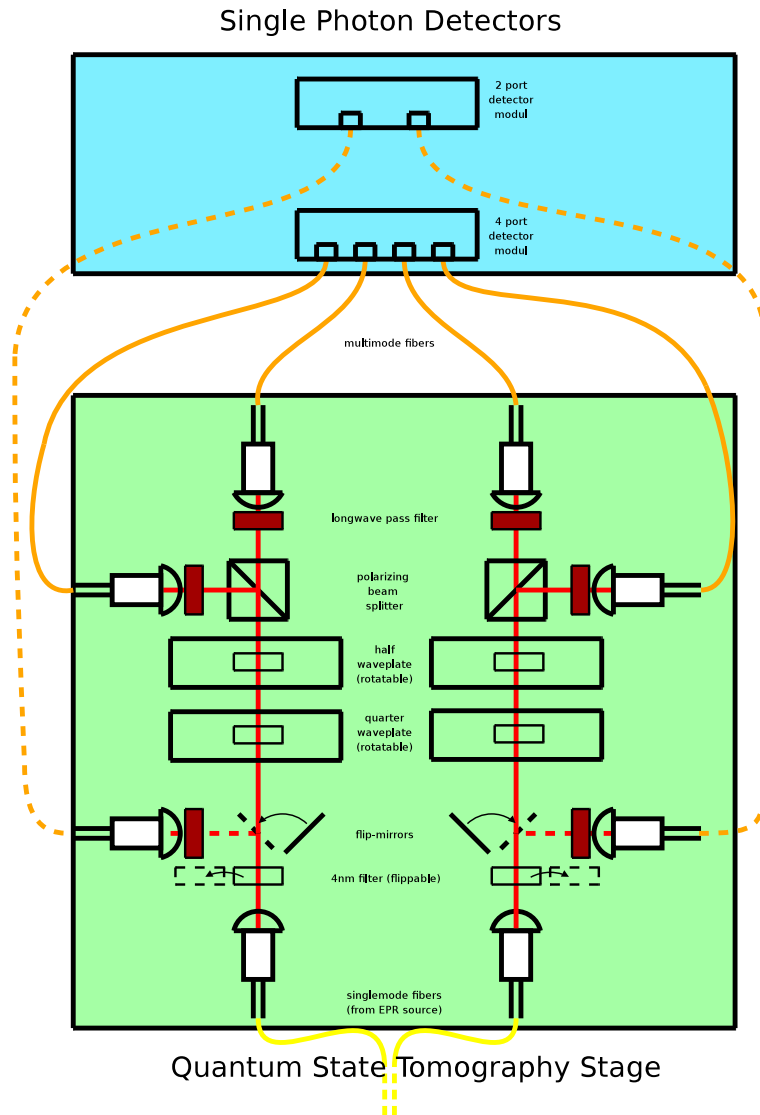


**FIGURE 39:** *Design of the quantum tomography stage as used for our measurements*

### 4.3.2 Motorized rotation stages

We again decided to use stepper motor controlled stages because they are very easy to control, have nearly no hysteresis and provide a very good reproducibility. Using the rotation stage 8MR151 from Standa (see figure (40)) also allows us to use the same motor driver that we use for the automated coupling system. Additionally it supports a very high rotation speed and the resolution is far enough for our needs. The serial protocol is also the same, which makes it possible to reuse the low-level drivers, too. Only the high-level drivers that provide absolute positioning needed some small adaptations. I will now describe the needed drivers in detail:

The low level driver is implemented as a very simple `expect` script. `Expect` is a tool that sends data to a (serial) terminal and checks the reply for validity. It simply allows to specify timeouts as well as to define error cases in the case of a wrong reply. So we only had to assemble a list of all available commands and their correct reply.

The high-level driver that I already mentioned is now needed to implement some features that the electrical driver itself does not support. In our case the electrical driver only supports relative motion about a

number of steps. But for practical use it would be essential to also allow absolute positioning. And additionally it should be possible to specify positions in degrees and not in a number of steps in order to avoid careless mistakes. And this is exactly what the high-level driver does.

In order to achieve reproducible absolute positioning one needs to have a reproducible initial position. Fortunately the rotation stage is equipped with an optical limit-switch that allows to reset to a fixed position. After the reset the high-level driver has to store the absolute position in a logfile in order to calculate the number of steps it has to go in order to reach the next position. As an optimization it also chooses the smallest path to the new position. For example if you want to go from  $0^\circ$  to  $350^\circ$  it will only move 10 counterclockwise instead of  $350^\circ$  clockwise.

Absolute positioning is the default operation but sometimes you also will want to do some relative motion. One example for this is an initial offset that you can specify to the individual stages. This can be very helpful if you mount waveplates or the like to the rotary stages and it is not possible to perfectly align them to the scale of the stage. But now you can simply do a test measurement in order to determine the offset to the correct alignment and then do a relative motion in order to correct this offset. This is the way we used to adjust our waveplates as you can see in the following section.

<b>Model</b>	8MR151
Rotation range	$360^\circ$
Resolution (full step)	0.6 arcmin
Resolution (1/8 step)	4.5 arcsec
Wobble	0.6 arcmin
Rotation speed	$50^\circ/s$
Weight	0.56kg

**TABLE 10:** *Rotation Stage*



**FIGURE 40:** *Standa 8MR151 rotation stage*

### 4.3.3 Waveplate adjustment

I already mentioned that the adjustment of the waveplates relative to the scale of the rotary stage is a difficult task. In our case we additionally had the problem that we had to use waveplates without mounting and therefore had no indication where the optical axes are. We could first do a classical measurement of the mounted waveplates, mark the optical axis and then try to align the axis to the scale as good as possible. But a more comfortable solution is to simply mount the waveplate to the rotary stage and do the alignment measurement within the final measurement setup.

This was put into practice by adding a polarizer directly after the single mode fiber. Without the waveplates the polarizer is adjusted in a way that the number of photons passing the PBS is maximized. If we would now add a waveplate with its optical axis parallel to this polarization it would have no influence. In order to determine the location of the optical axis we let the waveplate rotate by  $360^\circ$  and measure the photon rate at every  $2^\circ$ . In order to get unique values we only add one waveplate to the path at a time.

We got the following results for the half (see figure (41)) as well as quarter waveplate (see figure (42)) on Alice's side:

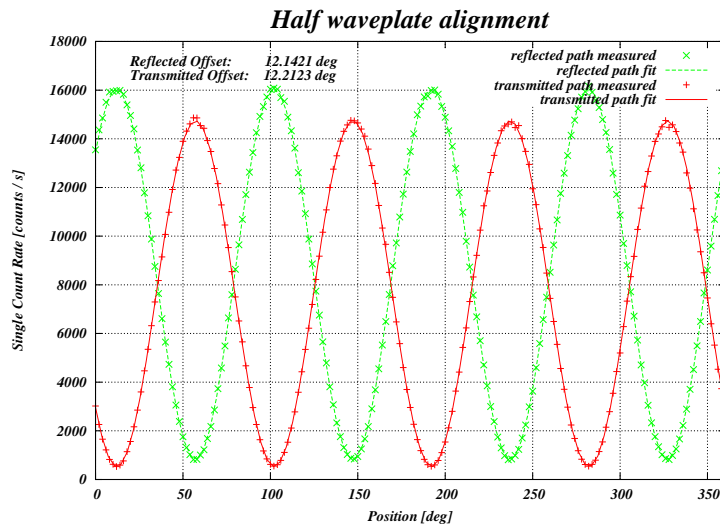


FIGURE 41: Offset measurement of half waveplate on Alice's side

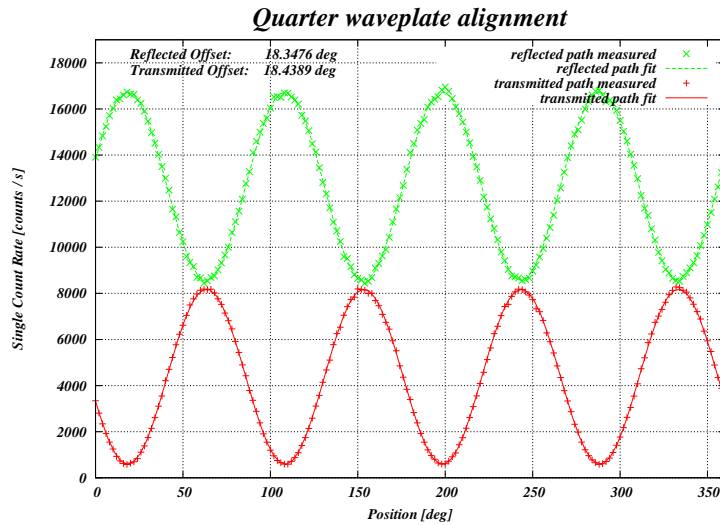


FIGURE 42: Offset measurement of quarter waveplate on Alice's side

As expected the half waveplate shows that periodic minima and maxima in both paths, the transmitted and the reflected. The different amplitude of both paths is an indication of a different measurement efficiency which consists of detector efficiency, coupling efficiency, included filters as well as the influence of the PBS. In contrast to this the quarter waveplate show oscillations between minimum and half of the maximum on one path and between maximum and half of the maximum on the other. The point where the photons are evenly distributed on both paths is where the optical axis of the quarter waveplate is oriented at  $45^\circ$  in contrast to the incoming polarization. In this case the light after the waveplate will be circular polarized and thus split up into two equal parts at the PCS. We also see that the calculated offset values of both paths match up to a tenth of a degree, which tells us that this measurement is reliable and very accurate.

The fact, that we could do the adjustment of the waveplates inside the final measurement system is due to the automation of the measurement system itself. So it was the first task where it helped to produce more accurate results with less effort. Now that the waveplate are aligned you can simple choose a measurement bases by rotating the waveplates to corresponding angles.

## 4.4 Analysis software

In order to get a very flexible software tool and also because we still have to test the behaviour of the software parts we implemented a modular system that consists of a backend that acquires the raw data as well as a frontend that does the quantum state reconstruction. Now we will describe these two components in depth and how they are linked together:

### 4.4.1 Data acquisition

In order to reconstruct the full quantum state of the photon pairs, one needs to do several consecutive measurements in different bases. So the first part of the analysis software is to start these measurements and acquire the raw data. In our implementation this task is done by a sequence file. There is one line with the four angles of the waveplates per measurement that should be started. This file is then read line by line from the toplevel script, the waveplates are rotated to the corresponding angles and the count rates are measured. Additionally the following abbreviations are replaced before interpretation of the toplevel script (see table (11)):

abbreviation	name	half waveplate angle	quarter waveplate angle
H	horizontal	$0^\circ$	$0^\circ$
V	vertical	$45^\circ$	$0^\circ$
D	diagonal	$22.5^\circ$	$0^\circ$
A	anti-diagonal	$-22.5^\circ$	$0^\circ$
R	right circular	$0^\circ$	$45^\circ$
L	left circular	$0^\circ$	$-45^\circ$

**TABLE 11:** *Abbreviations that can be used in the sequence file*

These abbreviations simplify the work with default bases but the sequence file itself allows to specify any angle for the waveplates that you want.

As a little additional feature I also implemented a version of the acquisition part that can be executed remotely over a network connection. Since all scripts are Linux shell scripts it is not a problem to run them remotely by using the `ssh` command. This for example allows to do the data acquisition on an inefficient lab PC whereas the time consuming calculations are done on a workstation controlled from your office.

Another possibility to do data acquisition is to simply read the raw count rates from a file. This method is especially helpful to reconstruct old measurements or to use data from external measurements. In this case

you only have to know the format of the raw data file and you can utilize all the features that the front end of the software provides.

#### 4.4.2 Computation

Fortunately there are already some tools available that can be used as our frontends. We decided to use these tools without any modifications in a first run. Within this project it was possible to link the front-end to our automated data acquisition and thus to do a completely automated quantum-state-tomography. But there was not enough time to really test the behaviour of the individual software tools. So we cannot yet tell which is the best tool, but the plan is to work out the most helpful features of all the tools and then implement one tool that combines all the advantages of the available tools. It follows a list of the used tools and the advantages and disadvantages that they bring along:

- **Online script from Paul Kwiat's Quantum Information Group:**

The script can be found at [23]. The homepage itself is also very interesting and offers a lot of additional information about quantum-state-tomography. We test this online version because it would be very interesting for the future to have one common place to analyze raw data from different workgroups from all over the world. This would guarantee that everyone uses the same sourcecode version and uses exactly the same definitions and corrections. Unfortunately the current version of the online script is not meant for a large number of consecutive calculations, but nevertheless it offers anybody the possibility to do a fast first check of his raw data and also allows to compare different measurements.

The software can handle different acquisition sequences. Since we have 16 degrees of freedom in our density matrix we need 16 measurements for a full specifications. If you use two detectors per side you have the possibility to combine some measurements and this will result in a sequence with only 9 consecutive measurements. The most precise tomography for a fixed number of total input pairs can be reconstructed for a sequence of 36 measurements using the full canonical basis  $(H, V, D, A, R, L) \otimes (H, V, D, A, R, L)$ . For more information about this see [24].

The tool also offers a possibility to consider some imperfections of the measurement system itself and correct the raw data before analysis. This allows to make the results more general because the influence of the measurement system can be reduced. For example one can subtract out the accidental coincidences due to a finite coincidence window. Another correction that can be of use when using a PBS and two detectors per side is a crosstalk correction, which solves the problem that the PBS reflects some fraction of the photons that it should have transmitted and vice versa. The last correction that the software provides is a drift compensation which is only needed if the source is not very stable and so the number of produced pairs changes significantly during the measurement sequence.

- **Offline version of the above script:** We also implemented an offline version because it is not always possible that you have access to the internet from your lab PC. An additional criterion was the faster execution time if the script is executed on a local machine. In this way we also have the possibility to look at the source code and do some modifications. The original script runs under `Matlab`, which makes it a bit complicated to automate the setup. Thus I ported the script to `octave` which is an open-source clone of `Matlab` and is in theory source code compatible. The only thing that I had to change is the Levenberg-Marquardt optimization algorithm `lsqnonlin` which I replaced by an opensource equivalent. One problem that we are still facing is that there is no plotting command available that allows to plot 3D bar diagrams. Thus we currently only get a text based output of the density matrix.
- **Mathematica script from the Quantum Information Group of the Vienna University:** Although this script is written for `Mathematica` it is very easy to execute the calculation from commandline and redirect its output into files. One problem is that `Mathematica` is commercial software and thus you need a license for each PC that it runs on. But on the other hand it offers a huge number of features and is also quite fast in execution.

The script itself does the following calculations. First of all it runs a maximum likelihood quantum state tomography algorithm. This yields a physical density matrix, but is not yet the end of the story. The next step is to allow local unitary transformations and Alice's and Bob's side which adds

new variables to the density matrix. The software allows you to specify the ideal state that you would like to get and then runs an optimization algorithm which determines the free parameters so that the resulting state is as much equal to the ideal state as possible. In practice these local unitary transformations could be implemented using some fiber based polarization controllers. `Mathematica` offers very powerful graphical commands that allow to create some nice 3D bar diagrams from the calculated densities. Additionally some entanglement measures are calculated in order to allow a fast comparison of different measures.

An extra feature that is implemented is a Montecarlo error estimation algorithm that allows to provide a standard deviation with your measuring results and not only the mean values. Unfortunately it is currently very slow and therefore we did not use this feature for our automated setup. But anyhow it will be interesting to think about it for future versions of the analysis software.

In the final setup this tool was the default tool that we use for data analysis due to the following reasons:

- **Execution time** is very fast.
- It plots **3D bar diagrams**.
- **Local unitary transformations** are very helpful since you do not have to fine tune the polarization controller before every measurement.



## 4.5 Measurements

### 4.5.1 Aligned system

Figure (43) shows a sample measurement of the adjusted source. In order to compensate the polarization rotation of the single-mode fiber we had to add a polarization controller. In this way the influence can be compensated directly in the hardware which would also be required if using the entangled photon pairs for some experiments. But this also means that from time to time or especially if the fiber was touched we have to do readjustment of the fiber controller. Due to the use of the polarization controller we can directly reproduce the correct density matrix and we need no additional virtual unitary transformations. Therefore figure (44) does not change significantly.

The single measurement period was chosen 4s, which lead to a total measurement time of about 49s. This contains the sequence of 9 consecutive measurement each lasting 4s and the time needed for the adjustment of the waveplates and the data analysis.

Finally table (12) summarized the calculated entanglement measures for the reconstructed density matrix.

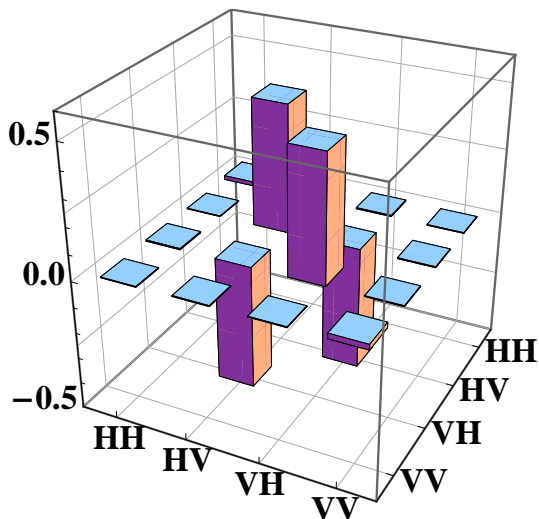


FIGURE 43: *Density matrix of the aligned source without correction*

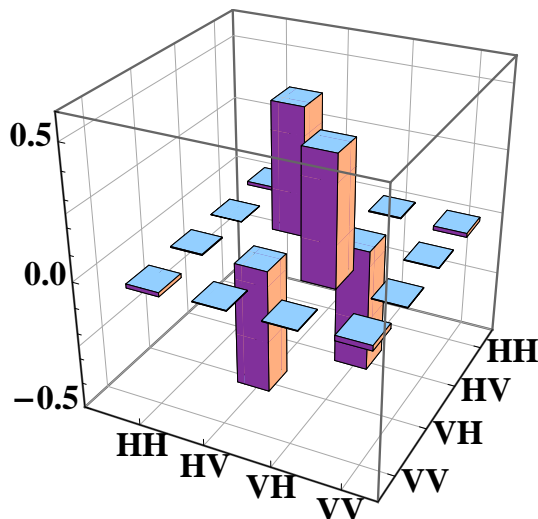


FIGURE 44: *Density matrix of the aligned source using local unitary transformation as further correction. Since the polarization controller is already adjusted this does not differ too much from the uncorrected state.*

<b>Fidelity</b>	96.5%
<b>Purity</b>	93.2%
<b>Linear Entropy</b>	0.090
<b>Tangle</b>	87.6%
<b>MaxS</b>	2.73

TABLE 12: *List of Entanglement measures calculated from the upper density matrix*

### 4.5.2 Misaligned system

Another possibility to compensate the influence of the fiber is to use the software feature that allows us to apply some virtual local unitary transformations. In order to demonstrate this feature we intentionally misaligned the fiber polarization controller and checked whether the original state is reconstructed. So figure (45) shows the matrix that we get from a direct reconstruction of the measurement results. This is actually the same state as before but with a misaligned polarization controller. Optimizing the state using virtual local unitary transformations lead to figure (46) which almost looks like the original state. The big advantage of this software compensation is that we do not have to adjust the polarization controller any longer. The calculated entanglement measures are given in table (13).

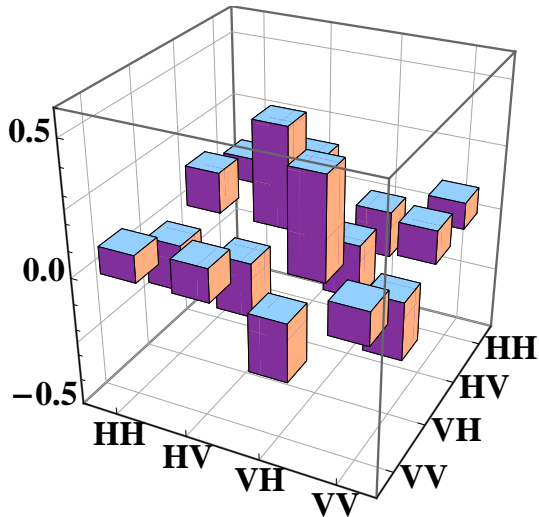


FIGURE 45: Density matrix with misaligned polarization controller without correction

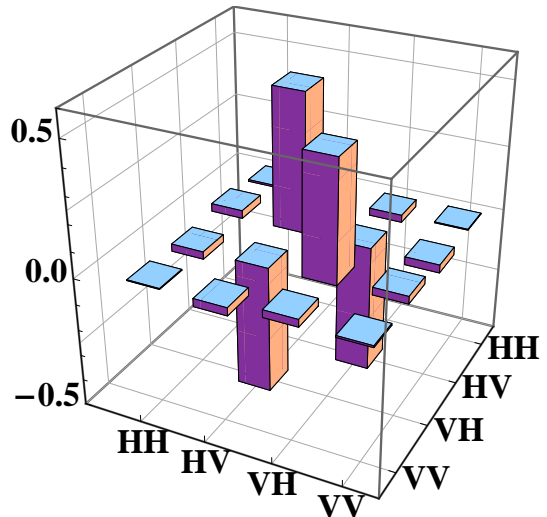


FIGURE 46: Density matrix with misaligned polarization using local unitary transformation as a correction

<b>Fidelity</b>	97.9%
<b>Purity</b>	94.5%
<b>Linear Entropy</b>	0.040
<b>Tangle</b>	91.8%
<b>MaxS</b>	2.77

TABLE 13: List of Entanglement measures calculated from the upper density matrix

## 4.6 Future development

- The hardware setup itself cannot be changed very much in the future. Perhaps the components itself will become smaller or one will give up some features of the current system. One additional feature that might be implemented in the future is an automated polarization controller. Such a system was already used for entanglement experiments over long fibers. It works with classical laser pulses that are sent over the same fiber in between the normal single photon operation. During this classical pulse the single photon detectors are switched off and a classical polarimeter is used to measure the influence of the fiber. A piezo fiber controller is then used to cancel the effect of the fiber. In fact it will not be very difficult to implement this for our state-tomography system.

- As already mentioned we just tested some available tools for data analysis. A future step would be to collect the helpful features of all tools in one application. Additional corrections should be implemented that allow to correct implementation specifics of different measurement systems. This would allow an accurate comparison of different results and an absolute statement about the quality of the measured system. Additionally it would make it possible to focus development efforts and avoid that different workgroups implement many different analysis tools at their own.
- If single photon detectors become smaller and cheaper in the near future it would be possible to build an online state tomography system that works like current polarimeters, but instead of using classical diodes they use single photon detectors. Each side would consist of 6 detectors (2 for each base) as well as 3 PBS (one for each base) and 2 ordinary beam splitters that randomly choose the current measurement base.

Together with a software that is able to correct the influence of the fiber this allows to build a measurement system without any moving parts, which would make it very stable. Due to higher count rates the measurement will also be very fast and you will be able to watch the diagram during source adjustment.

## 5 Conclusion

The following subsection summarize the results and the lessons that we learned during the implementation of the individual parts of the project.

### 5.1 Laser system

The first part that we re-implemented was the laser system. The usage of a cage system proved very useful since it leads to a very stable and compact system. The degrees of freedom can be reduced by using adjustment aids for the initial adjustment and only maintain those degrees of freedom really needed during operation. The use of round cylindrical lenses allows to mount them using default cage mounts which also simplified the system a lot.

The use of an unstabilized diode laser has the consequence that the center wavelength is shifted in comparison with the design wavelength. Of course this could be solved by adapting filters and other wavelength dependent components to this new wavelength. But for a stable operations this would require some additional measurement of the long time behaviour of this wavelength shift. Additionally we realized that the usage of the power control feature of the laser leads to an additional offset. So although the advantages of compact size, low acquisition costs and easy handling are noted changing to a stabilized laser would be worth consideration for future projects.

### 5.2 Beam control

The control loop works very well and allows to eliminate the dependence of the pump beam emission angle on the external temperature. This allows to use the source outside of laboratory for practical experiments. As we saw from our measurements the accuracy of the piezo-mirror-mount is sufficient for our needs and the used detection scheme is able to resolve individual steps of the piezo motor.

The usage of a 14bit ADC would allow to use the measured data without averaging, but this is not really important for the final system.

### 5.3 Walkoff compensation

The usage of only one compensation crystal directly behind the first BBO reduces system size and saves the costs of one crystal. Our measurements showed no significant difference in the single- as well as coincidence-rates.

## 5.4 Coupling system

The coupling system using 2 lenses in order to decouple translational and tilt degrees of freedom has proven very useful for an easy source adjustment. And it is also a first step towards a fully automated coupling system. Unfortunately we could not realize this automation due to a lack of time. But the system's design should make it easy to simply replace the manual stages by motorized ones. All one then needs to do is to implement the control algorithm for the coupling stabilization. If an automation of the initial adjustment is also possible depends on the accuracy of the pre-adjustment and the catchment area of the control system.

The use of default fiber collimators for fiber coupling fixes another degree of freedom and allows to simply select the divergence angle of the beam that should be mapped to the acceptance mode of the single mode fiber.

## 5.5 Quantum state tomography

The implementation of the mechanical part of the system was straight forward. The rotation stages work perfectly and fit all our needs. The adjustment of the waveplates that could be done within the final setup demonstrates a further simplification that was implemented.

The mechanical measurement system can be used in conjunction with three different software tools for data analysis that provide different capabilities. The compensation of local unitary transformation allows measure the state of the source without the need for fiber polarization controllers that compensate the influence of the single mode fiber. Compensation of some imperfection of the measurement system itself should result in more objective measurement results.

In order to measure the actual count rates we switched to a time-tagging system that provides some additional capabilities. The most important one is that duration differences due to different path lengths can simply be compensated in software. Additionally it allows to display photon statistics and for example to detect time shift attacks.

## Appendix

### A Example calculation with MAPLE

The following example should demonstrate how to use ABCD matrices to calculate lens systems. In this simple case we take an given input beam and want to focus it to a beam waist of  $w_f = 100\mu m$ . In order to archive this we try two different systems. The first only uses one single lens whereas the second one consists of two lenses. Finally this calculation will show us that using two lenses allows to build a smaller system.

First we start with a measurement of the input beam. It is characterized by its wavelength  $\lambda_0$ , its Rayleigh range  $z_0$ , the focus position  $d_0$  and the beam quality parameter  $M_0$ . These parameters are used to get a formula for the input beam  $q_0$ .

In the next step we apply some ABCD matrices to this input beam in order to model the general setup of the lens system. We use variables for all unknown values.  $L_i$  for the lens' positions,  $f_i$  for the lens' focal lengths,  $d_i$  for the focus positions,  $z_i$  for the Rayleigh ranges and  $w_i$  for the beam waists. We also determine the values of some of the variables in this step in order to reduce the number of degrees of freedom of the system. For example the position of the first lens should be 10cm after the laser output.

After the general lens system setup is defined the actual calculation can be done. We define our constraints and solve the corresponding equations. Finally we see that using a single lens leads to a focus position 66cm after the laser output whereas two lenses can reduce the distance to only 28cm.

#### A.1 Include Packages

```
> restart:
> with(Statistics):
> with(plots):
> with(LinearAlgebra):
> with(Optimization):
```

Warning, the name `changecoords` has been redefined

Warning, the name `Rank` has been rebound

Warning, the assigned name `Interactive` now has a global binding

#### A.2 Function Definitions

```
> omega := (q, lambda, M) -> M * sqrt(-lambda/pi * Im(1/q)**(-1)):
> ABCD := (q, X) -> (X[1,1] * q + X[1,2]) / (X[2,1] * q + X[2,2]):
> L := f -> Matrix(2, 2, [[1,0], [-1/f,1]]):
```

#### A.3 Initial Beam

```
> lambda0 := 405E-9:
> M0 := 1.80208579416017156:
> z0 := 4.67719103252808832:
> d0 := 6.42473084447338127:
> q0 := z -> z - d0 + I * z0:
```

#### A.4 Direct map

```
> assume(f1, real):
> assume(d1, real):
> M1 := M0:
> L1 := 0.10:
```

```

> q1 := z -> ABCD(q0(L1), L(f1)) + z - L1:
> eq1 := Re(q1(d1)) = 0:
> d1 := solve(eq1, d1):
> z1 := Im(q1(d1)):
> w1 := evalf(omega(q1(d1), lambda0, M1)):

```

## A.5 Map with intermediate focus

```

> assume(d2b, real):
> assume(d2a, real):
> assume(L2b, real):
> M2 := M0:
> L2a := 0.10:
> q2a := z -> ABCD(q0(L2a), L(f2a)) + z - L2a:
> eq2a := Re(q2a(d2a)) = 0:
> d2a := solve(eq2a, d2a):
> z2a := Im(q2a(d2a)):
> w2a := evalf(omega(q2a(d2a), lambda0, M2)):
> q2b := z -> ABCD(q2a(L2b), L(f2b)) + z - L2b:
> eq2b := Re(q2b(d2b)) = 0:
> d2b := solve(eq2b, d2b):
> z2b := Im(q2b(d2b)):
> w2b := evalf(omega(q2b(d2b), lambda0, M2)):

```

## A.6 Calculation

```

> wf := 100E-6:
> f1res := solve(w1 = wf, f1)[1]
> d1res := eval(d1, f1 = f1res)

f1res := 0.5969864169

d1res := 0.6616377804

> f2a := 0.050:
> f2b := 0.010:
> L2bres := solve(w2b = wf, L2b)[2]
> d2bres := eval(d2b, L2b = L2bres)

L2bres := 0.1606099907

d2bres := 0.2810637005

```

## B Setup HowTo for Agilis controller AG-UC2

I wrote the following howto to setup the AG-UC2 controller under Linux. I also provided these information to Newport which sell Agilis products to put it on their homepage.

### B.1 setup\_howto.txt

Setup Howto for Agilis AG-UC2 Controller:

This short howto should describe how to get the AG-UC2 controller to work with a default Linux system. Despite the fact that there is no special Linux driver offered for this device it is no problem to make it work because it uses a default USB to serial converter chip from FTDI Chip. Thus it is possible to use the generic `ftdi_sio` Linux driver which is included since 2.4.30 I think. The following description is tested under a default Debian Lenny installation with a 2.6.26-1-686 Linux kernel. All tools that we used can simply be install using `apt` (`apt-get install minicom expect`).

The first thing that you have to find out is the USB device and vendor ID of your device. Therefor you have to plug in your device and use `'lsusb'` to show what devices are connected to your PC:

```
> lsusb
Bus 005 Device 001: ID 1d6b:0002 Linux Foundation 2.0 root hub
Bus 003 Device 002: ID 104d:3000
Bus 003 Device 003: ID 05e3:0604 Genesys Logic, Inc. USB 1.1 Hub
Bus 003 Device 001: ID 1d6b:0001 Linux Foundation 1.1 root hub
```

The second line shows that our device has a vendor ID `0x1D6B` and a device ID `0x3000`. (Plug and unplug the device if you are not sure which line belongs to the AG-UC2). The next step is load the FTDI driver and specify the correct IDs:

```
> sudo modprobe ftdi_sio vendor=0x104D product=0x3000
```

Run `dmesg` in order to verify that everything worked as expected:

```
> dmesg
[ 3054.054454] usb 3-1: new full speed USB device using uhci_hcd and address 13
[ 3054.249384] usb 3-1: configuration #1 chosen from 1 choice
[ 3054.256694] usb 3-1: New USB device found, idVendor=104d, idProduct=3000
[ 3054.256704] usb 3-1: New USB device strings: Mfr=1, Product=2, SerialNumber=3
[ 3054.256709] usb 3-1: Product: Agilis
[ 3054.256713] usb 3-1: Manufacturer: Newport
[ 3054.256717] usb 3-1: SerialNumber: FTRWR9V6
[ 3112.702518] usbserial: USB Serial support registered for FTDI USB Serial Device
[ 3112.702518] ftdi_sio 3-1:1.0: FTDI USB Serial Device converter detected
[ 3112.702518] ftdi_sio: Detected FT232RL
[ 3112.702518] usb 3-1: FTDI USB Serial Device converter now attached to ttyUSB4
[ 3112.702518] usbcore: registered new interface driver ftdi_sio
[ 3112.702518] ftdi_sio: v1.4.3:USB FTDI Serial Converters Driver
```

This output shows that the driver loaded successful as well as that a new USB serial device was found and attached to `/dev/ttyUSB4`. Now that we have this the only thing we have to do is to adjust COM settings and send commands to the controller. In order to find the right settings I normally use `'minicom'` first. Look at the manpages if you don't know how to

adjust settings. This is the configfile that I used to talk to the AG-UC2 controller:

```
# Machine-generated file - use setup menu in minicom to change parameters.
pu port          /dev/ttyUSB4
pu baudrate     921600
pu bits         8
pu parity       N
pu stopbits     1
pu rtscts       No
```

If you prefer stty for example to use in shell scripts the following command will also work:  
> stty -F /dev/ttyUSB4 921600 cs8 -parenb -cstopb -crtscts

Now everything is set up and you can send commands to the AG-UC2 controller. In my case I use a simple expect script to handle this task. It reads commands either from stdin or from the commandline. The first commandline parameter is interpreted as port if it starts with /dev. In this version it is not checked whether there is a correct reply from the controller.

The expect script can be found in the file AG\_UC2\_cmd.

So the rest is up to you. I want to thank all other developers that made it possible to use this controller under Linux and hope that Linux support for other Newport products will follow this role model.

Florian Bruckner  
<florian.bruckner@ait.ac.at>

## B.2 AG\_UC2\_cmd expect scripts

```
#!/usr/bin/expect --

# AG_UC2_cmd commands
# (c) 2009 Florian Bruckner <florian.bruckner@arcs.ac.at>
#
# Simple Expect script that sends commands to AG-UC2 controller from
# Newport in order to control motorized stages.
#
# input is possible via commandline parameters or via stdin.
# first parameter will be handled as COM port if matching with ~/dev/.*$
#
# the next parameter could be "init" if the COM port should be initialized
# before usage. This leads to problems if process should be executed in
# background.
#
# if a command should give a reply then any reply is valid. Currently
# there is no check if it is the right reply for the current command.

set port "/dev/ttyUSB0"
set timeout 1
set cmds [list]

log_user 0
```



```

# check if first argument is a devicefile
set first [lindex $argv 0 ]
if { [ regexp "^/dev/.*$" $first match ] } {
set port $first
set argv [ lreplace $argv 0 0 ]
set argc [ expr $argc - 1 ]
}

# check if next argument is a init-flag
set first [lindex $argv 0 ]
if { [ regexp "^init$" $first match ] } {
stty -F $port 921600 cs8 -parenb -cstopb -crtscts
}

# handle following arguments
if { $argc < 1 } {
while { 1 } {
gets stdin this
if { [eof stdin] } { break }
lappend cmds $this
}
} else {
set cmds [ split $argv ]
}

spawn -open [open $port w+]

foreach cmd $cmds {
send "$cmd\r"

switch -regexp -- $cmd {
{^PH$} -
{^TE$} -
{^VE$} -
{^..?TP$} -
{^..?MA$} -
{^..?TS$} -
{[?]} {
expect {
timeout {
puts "[exec date "+%F %T"] $cmd timeout!"
exit -5
}
"\r"
}
puts $expect_out(buffer)
}
}
}
close

```

## References

- [1] A. Fedrizzi, *A Compact Source for Quantum Key Distribution*, University of Vienna, Institute of Atomic and Subatomic Physics (2004).
- [2] H. R. Böhm, *A Compact Source for Polarization Entangled Photon Pairs*, University of Vienna, Institute of Atomic and Subatomic Physics (2003).
- [3] B. E. A. Saleh, M. C. Teich, *Fundamentals of Photonics*, John Wiley & Sons, Inc. New York (1991).
- [4] D. Bouwmeester, A. Eckert, A. Zeilinger, *The Physics of Quantum Information*, Springer-Verlag Berlin Heidelberg (2000).
- [5] G. Reider, *Photonik*, Springer-Verlag Wien (2005).
- [6] R. Horodecki, P. Horodecki, M. Horodecki, K. Horodecki, *quant-ph/0702225* (2007).
- [7] V. Scarani, *quant-ph/0910.4222* (2009).
- [8] M. A. Nielsen, I. L. Chuang, *Quantum Computation and Quantum Information*, Cambridge University Press Cambridge (2000).
- [9] G. O. Myhr *Measures of entanglement in quantum mechanics*, Norwegian University of Science and Technology, Department of Physics (2004)
- [10] M. B. Plenio, S. Virmani, *quant-ph/0504163* (2006)
- [11] D. McHugh, M. Ziman, V. Buzek *quant-ph/0607012*, (2006)
- [12] W. K. Wootters, *Phys. Ref. Lett.* **80**, 2245 (1998)
- [13] M. A. Nielsen, *quant-ph/9606012*, (1996)
- [14] N. Gisin, G. Ribordy, W. Tittel, H. Zbinden, *Quantum cryptography*, Rev. Mod. Phys. **74**, 145 (2002)
- [15] M. Peev, et al., *The SECOQC quantum key distribution network in Vienna*, New J. Phys. **11**, 075001 (2009)
- [16] C. I. T. Schmid, *Kompakte Quelle verschränkter Photonen und Anwendungen in der Quantenkommunikation*, Ludwig-Maximilians-Universität München, Fakultät für Physik (2004).
- [17] Ch. Kurtsiefer, M. Oberparleiter, H. Weinfurter, *High efficiency entangled photon pair collection in type II parametric fluorescence*, Phys. Rev. A, **64**, 023802 (2001).
- [18] A. Poppe, et al., *Practical Quantum Key Distribution with Polarization-Entangled Photons*, Opt. Express **12**, 3865-3871 (2004), or *quant-ph/0404115*, (2004).
- [19] J. B. Altepeter, E. R. Jeffrey, P. G. Kwiat, *Photonic State Tomography*, [http://research.physics.illinois.edu/QI/Photonics/Tomography/tomography\\_theory/amo\\_tomo\\_chapter.pdf](http://research.physics.illinois.edu/QI/Photonics/Tomography/tomography_theory/amo_tomo_chapter.pdf) (Oct. 2009)
- [20] B. Blauensteiner, et al., *quant-ph/0810.4785*, (2009)
- [21] B. Qi, et al., *quant-ph/0512080*, (2006)
- [22] R. Ursin, et al., *Entanglement-based quantum communication over 144km*, Nature Physics **3**, 481-486 (2007)
- [23] Homepage of Paul Kwiat's Quantum Information Group, <http://webusers.physics.illinois.edu/~kwiat/TomographyDemo.php>, (2009)
- [24] J. B. Altepeter, et al., *Experimental Methods for Detecting Entanglement*, Phys. Rev. Lett. **95**, 033601 (2005)